Little is known about the role of G proteins and GPCRs in the life cycle and pathogenesis of HTLV-I. Studies have shown that CCR4[10] and CCR7[2] are frequently expressed in ATL cells, and chemokines, including MCP-1,[3] RANTES,[11] MIP-1α,[5] and SDF-1α,[18,28] have been shown to modulate migration and tissue localization of HTLV-I–infected cells. In addition, expression of the HTLV-I regulatory protein Tax in immortalized T-cell lines has been shown to be involved the activation of the SDF-1α/CXCR4 pathway.[29]

The present study has clearly demonstrated the cell surface expression of CXCR4 on leukemic cells, a specific chemotactic response to SDF-1α, and that cell migration is associated with MEK-ERK signaling. Following the interaction with SDF-1α, surface CXCR4 translocates to an intracellular compartment.[22] It has been demonstrated that the GPCR heteromultimerized with receptors of tyrosine kinases translocated to the endosome and promoted activation of endosomal Ras-ERK pathways in several cell types.[30] Thus, it is possible that the subcellular localization of CXCR4 in pML cells may also promote activation of additional signaling pathways, in addition to ERK1/2, and this is currently under investigation.

Our studies also demonstrated that the CXCR4 antagonist AMD3100 inhibited cell migration in response to SDF-1α. The MEK inhibitor U0126 was found to inhibit the chemotaxis of pML cells and also inhibited phosphorylation of ERK1/2. In contrast, AMD3100 although significantly suppressing the chemotactic activity of pML cells, had less impact on the phosphorylation of ERK1/2 compared with U0126 (Figure 2G-H and supplemental Figure 1). These results suggest that phosphorylation of ERK1/2 may also be regulated by other cellular factors. Indeed, it is likely that other signaling pathways and other processes are involved downstream of CXCR4. We also performed a Mouse Inflammatory Cytokine and Receptors Microarray analysis, in which 113 key genes are involved, to determine the possible role of other chemokine receptors (SABiosciences). Using pML cells and pan T cells derived from B6 mice, we could not observe any up-regulation of other chemokine receptors in pML cells. Thus, although the SDF-1α/CXCR4 pathway appears to be uniquely important, it is almost certain that other pathways also contribute to leukemic cell invasion, including cell adhesion molecules,[8,9] matrix metalloproteinases,[31] and other biomolecules.[32] Microarray data have been deposited to Gene Expression Omnibus (GEO) and can be found under accession numbers GSE17341, GSM433627, and GSM433628.[33]

The results obtained from our previous and the present studies also confirm that our murine models do accurately reproduce human disease in that, in addition to developing the clinical and pathologic features of ATL, we also demonstrated a dose-dependent promotion of chemotactic activity by SDF-1α, phosphorylation of ERK1/2, and an AMD3100 inhibition of SDF-1α–induced ERK1/2 phosphorylation and migration in primary human ATL cells.

SDF-1α is released from fibroblasts and is ubiquitously expressed in many tissues, including liver, kidney, and lung.[26] We confirmed SDF-1α mRNA expression in range of mouse tissues (Figure 4A) and that expression of SDF-1α may be associated with invasion of leukemic cells both in the mouse model and human disease.

AMD3100 is currently being evaluated in a phase 1 trial using healthy volunteers,[34] and in a phase 2 trial involving HIV-I–infected patients.[35] In addition, this drug is considered to be a promising candidate for the treatment of other disorders in which SDF-1α/CXCR4 interactions may be important, including rheumatoid arthritis,[36] breast cancer metastasis,[37] atherosclerosis, and asthma.[38] We demonstrated that AMD3100 inhibited infiltration of pML cells into liver and lung tissues in SCID mice but that the inhibitory effect was influenced by the number of inoculated pML cells. These results imply that when a large number of leukemic cells are used in the inoculation, this can overcome the inhibitory effect of AMD3100. This could be related to the levels of AMD3100, and may require more optimal dosing, or to other unknown factors. This is currently under investigation but our results prove in principle the role of AMD3100 in preventing infiltration of leukemic cells and support the findings of our in vitro experiments. Our studies also suggest that AMD3100 should be a considered as a candidate agent as part of combination therapy of ATL. It has been shown that a combination of α interferon with retrovir can produce significant remission in certain ATL patients,[39] and it is possible that the addition of AMD3100 could contribute to the efficacy of this combination. It is certainly likely that leukemic cell infiltration will involve other molecular mechanisms, and as such combination therapy in the future would also include inhibitors of these processes. Clinical trials in our murine model and ultimately in human disease will ascertain whether CXCR4 antagonists and other agents will play a role and/or contribute to treatment efficacy in combination therapeutic approaches.

Acknowledgments

We thank Ms S. Yamanouchi and Ms M. Sasada for technical assistance, and Drs T. Suzuki and Y. Makino for valuable suggestions.

Y.O. is a research fellow of the Japan Society for the Promotion of Science.

This study was supported in part by grants from the Ministry of Education, Culture, Sports, Science, and Technology; the Ministry of Health, Labor, and Welfare, Japan; the Japan Health Sciences Foundation; the Naito Foundation; the Takeda Science Foundation; and the Program of Founding Research Centers for Emerging and Reemerging Infectious Diseases, MEXT, Japan.

Authorship

Contribution: A.K., T.K., H.S., and H.H. designed research; H.H., H.S., and W.W.H. developed the ATL animal model; A.K., Y.O., and A.A. performed research; H.I., M.O., and T.O. contributed new reagents/materials; T.T. and T.S. contributed pathologic analysis; and A.K., W.W.H., H.S., and H.H. wrote the paper.

Conflict-of-interest disclosure: The authors declare no competing financial interests.

Correspondence: Hideki Hasegawa, Department of Pathology, National Institute of Infectious Diseases, 4-7-1 Gakuen, Musashimurayama City, Tokyo, Japan, 208-0011; e-mail: hasegawa@nih.go.jp; or Hirofumi Sawa, Department of Molecular Pathobiology, Research Center for Zoonosis Control, Hokkaido University, Sapporo, N20, W10, Kita-ku, Sapporo, Japan, 001-0020; e-mail: h-sawa@czc.hokudai.ac.jp.

References

1. Uchiyama T. Human T cell leukemia virus type I (HTLV-I) and human diseases. *Annu Rev Immunol.* 1997;15:15-37.

2. Matsuoka M. Human T-cell leukemia virus type I and adult T-cell leukemia. *Oncogene.* 2003; 22(33):5131-5140.

3. Mori N, Ueda A, Ikeda S, et al. Human T-cell leukemia virus type I tax activates transcription of the human monocyte chemoattractant protein-1

gene through two nuclear factor-kappaB sites. *Cancer Res.* 2000;60(17):4939-4945.

4. Imaizumi Y, Sugita S, Yamamoto K, et al. Human T cell leukemia virus type-I Tax activates human macrophage inflammatory protein-3 alpha/CCL20 gene transcription via the NF-kappa B pathway. *Int Immunol.* 2002;14(2):147-155.
5. Tanaka Y, Mine S, Figdor CG, et al. Constitutive chemokine production results in activation of leukocyte function-associated antigen-1 on adult T-cell leukemia cells. *Blood.* 1998;91(10):3909-3919.
6. Ruckes T, Saul D, Van Snick J, Hermine O, Grassmann R. Autocrine antiapoptotic stimulation of cultured adult T-cell leukemia cells by overexpression of the chemokine I-309. *Blood.* 2001; 98(4):1150-1159.
7. Shimauchi T, Imai S, Hino R, Tokura Y. Production of thymus and activation-regulated chemokine and macrophage-derived chemokine by CCR4+ adult T-cell leukemia cells. *Clin Cancer Res.* 2005;11(6):2427-2435.
8. Ishikawa T, Imura A, Tanaka K, Shirane H, Okuma M, Uchiyama T. E-selectin and vascular cell adhesion molecule-1 mediate adult T-cell leukemia cell adhesion to endothelial cells. *Blood.* 1993;82(5):1590-1598.
9. Tatewaki M, Yamaguchi K, Matsuoka M, et al. Constitutive overexpression of the L-selectin gene in fresh leukemic cells of adult T-cell leukemia that can be transactivated by human T-cell lymphotropic virus type 1 Tax. *Blood.* 1995;86(8): 3109-3117.
10. Campbell DJ, Kim CH, Butcher EC. Chemokines in the systemic organization of immunity. *Immunol Rev.* 2003;195:58-71.
11. Yoshie O, Imai T, Nomiyama H. Chemokines in immunity. *Adv Immunol.* 2001;78:57-110.
12. Nagasawa T, Nakajima T, Tachibana K, et al. Molecular cloning and characterization of a murine pre-B-cell growth-stimulating factor/stromal cell-derived factor 1 receptor, a murine homolog of the human immunodeficiency virus 1 entry coreceptor fusin. *Proc Natl Acad Sci U S A.* 1996; 93(25):14726-14729.
13. Bleul CC, Fuhlbrigge RC, Casasnovas JM, Aiuti A, Springer TA. A highly efficacious lymphocyte chemoattractant, stromal cell-derived factor 1 (SDF-1). *J Exp Med.* 1996;184(3):1101-1109.
14. Lee BC, Lee TH, Avraham S, Avraham HK. Involvement of the chemokine receptor CXCR4 and its ligand stromal cell-derived factor 1alpha in breast cancer cell migration through human brain microvascular endothelial cells. *Mol Cancer Res.* 2004;2(6):327-338.
15. Yoshie O, Fujisawa R, Nakayama T, et al. Frequent expression of CCR4 in adult T-cell leukemia and human T-cell leukemia virus type 1-transformed T cells. *Blood.* 2002;99(5):1505-1511.
16. Mori N, Krensky AM, Ohshima K, et al. Elevated expression of CCL5/RANTES in adult T-cell leukemia cells: possible transactivation of the CCL5 gene by human T-cell leukemia virus type I tax. *Int J Cancer.* 2004;111(4):548-557.
17. Hasegawa H, Nomura T, Kohno M, et al. Increased chemokine receptor CCR7/EBI1 expression enhances the infiltration of lymphoid organs by adult T-cell leukemia cells. *Blood.* 2000;95(1): 30-38.
18. Nagakubo D, Jin Z, Hieshima K, et al. Expression of CCR9 in HTLV-1+ T cells and ATL cells expressing Tax. *Int J Cancer.* 2007;120(7):1591-1597.
19. Hasegawa H, Sawa H, Lewis MJ, et al. Thymus-derived leukemia-lymphoma in mice transgenic for the Tax gene of human T-lymphotropic virus type I. *Nat Med.* 2006;12(4):466-472.
20. Hatse S, Princen K, Bridger G, De Clercq E, Schols D. Chemokine receptor inhibition by AMD3100 is strictly confined to CXCR4. *FEBS Lett.* 2002;527(1-3):255-262.
21. Colmone A, Amorim M, Pontier AL, Wang S, Jablonski E, Sipkins DA. Leukemic cells create bone marrow niches that disrupt the behavior of normal hematopoietic progenitor cells. *Science.* 2008;322(5909):1861-1865.
22. Neel NF, Schutyser E, Sai J, Fan GH, Richmond A. Chemokine receptor internalization and intracellular trafficking. *Cytokine Growth Factor Rev.* 2005;16(6):637-658.
23. Ganju RK, Brubaker SA, Meyer J, et al. The alpha-chemokine, stromal cell-derived factor-1alpha, binds to the transmembrane G-protein-coupled CXCR-4 receptor and activates multiple signal transduction pathways. *J Biol Chem.* 1998;273(36):23169-23175.
24. Peng SB, Peek V, Zhai Y, et al. Akt activation, but not extracellular signal-regulated kinase activation, is required for SDF-1alpha/CXCR4-mediated migration of epitheloid carcinoma cells. *Mol Cancer Res.* 2005;3(4):227-236.
25. Alsayed Y, Ngo H, Runnels J, et al. Mechanisms of regulation of CXCR4/SDF-1 (CXCL12)-dependent migration and homing in multiple myeloma. *Blood.* 2007;109(7):2708-2717.
26. Tashiro K, Tada H, Heilker R, Shirozu M, Nakano T, Honjo T. Signal sequence trap: a cloning strategy for secreted proteins and type I membrane proteins. *Science.* 1993;261(5121):600-603.
27. Kukreja P, Abdel-Mageed AB, Mondal D, Liu K, Agrawal KC. Up-regulation of CXCR4 expression in PC-3 cells by stromal-derived factor-1alpha (CXCL12) increases endothelial adhesion and transendothelial migration: role of MEK/ERK signaling pathway-dependent NF-kappaB activation. *Cancer Res.* 2005;65(21):9891-9898.
28. Moriuchi M, Moriuchi H, Fauci AS. HTLV type I Tax activation of the CXCR4 promoter by association with nuclear respiratory factor 1. *AIDS Res Hum Retroviruses.* 1999;15(9):821-827.
29. Twizere JC, Springael JY, Boxus M, et al. Human T-cell leukemia virus type-1 Tax oncoprotein regulates G-protein signaling. *Blood.* 2007; 109(3):1051-1060.
30. Mor A, Philips MR. Compartmentalized Ras/MAPK signaling. *Annu Rev Immunol.* 2006;24: 771-800.
31. Mori N, Sato H, Hayashibara T, et al. Human T-cell leukemia virus type I Tax transactivates the matrix metalloproteinase-9 gene: potential role in mediating adult T-cell leukemia invasiveness. *Blood.* 2002;99(4):1341-1349.
32. Hayashibara T, Yamada Y, Miyanishi T, et al. Vascular endothelial growth factor and cellular chemotaxis: a possible autocrine pathway in adult T-cell leukemia cell invasion. *Clin Cancer Res.* 2001;7(9):2719-2726.
33. National Center for Biotechnology Information. Gene Expression Omnibus (GEO). http://www.ncbi.nlm.nih.gov/geo. Accessed July 28, 2009.
34. Hendrix CW, Flexner C, MacFarland RT, et al. Pharmacokinetics and safety of AMD-3100, a novel antagonist of the CXCR-4 chemokine receptor, in human volunteers. *Antimicrob Agents Chemother.* 2000;44(6):1667-1673.
35. Hendrix CW, Collier AC, Lederman MM, et al. Safety, pharmacokinetics, and antiviral activity of AMD3100, a selective CXCR4 receptor inhibitor, in HIV-1 infection. *J Acquir Immune Defic Syndr.* 2004;37(2):1253-1262.
36. Nanki T, Hayashida K, El-Gabalawy HS, et al. Stromal cell-derived factor-1-CXC chemokine receptor 4 interactions play a central role in CD4+ T cell accumulation in rheumatoid arthritis synovium. *J Immunol.* 2000;165(11):6590-6598.
37. Müller A, Homey B, Soto H, et al. Involvement of chemokine receptors in breast cancer metastasis. *Nature.* 2001;410(6824):50-56.
38. Abi-Younes S, Sauty A, Mach F, Sukhova GK, Libby P, Luster AD. The stromal cell-derived factor-1 chemokine is a potent platelet agonist highly expressed in atherosclerotic plaques. *Circ Res.* 2000;86(2):131-138.
39. Bazarbachi A, Nasr R, El-Sabban ME, et al. Evidence against a direct cytotoxic effect of alpha interferon and zidovudine in HTLV-I associated adult T cell leukemia/lymphoma. *Leukemia.* 2000; 14(4):716-721.

nature

Vol 459|4 June 2009|doi:10.1038/nature07969

LETTERS

Frequent inactivation of A20 in B-cell lymphomas

Motohiro Kato[1,2], Masashi Sanada[1,5], Itaru Kato[6], Yasuharu Sato[7], Junko Takita[1,2,3], Kengo Takeuchi[8], Akira Niwa[6], Yuyan Chen[1,2], Kumi Nakazaki[1,4,5], Junko Nomoto[9], Yoshitaka Asakura[9], Satsuki Muto[1], Azusa Tamura[1], Mitsuru Iio[1], Yoshiki Akatsuka[11], Yasuhide Hayashi[12], Hiraku Mori[13], Takashi Igarashi[2], Mineo Kurokawa[4], Shigeru Chiba[3], Shigeo Mori[14], Yuichi Ishikawa[8], Koji Okamoto[10], Kensei Tobinai[9], Hitoshi Nakagama[10], Tatsutoshi Nakahata[6], Tadashi Yoshino[7], Yukio Kobayashi[9] & Seishi Ogawa[1,5]

A20 is a negative regulator of the NF-κB pathway and was initially identified as being rapidly induced after tumour-necrosis factor-α stimulation[1]. It has a pivotal role in regulation of the immune response and prevents excessive activation of NF-κB in response to a variety of external stimuli[2–7]; recent genetic studies have disclosed putative associations of polymorphic *A20* (also called *TNFAIP3*) alleles with autoimmune disease risk[8,9]. However, the involvement of A20 in the development of human cancers is unknown. Here we show, using a genome-wide analysis of genetic lesions in 238 B-cell lymphomas, that *A20* is a common genetic target in B-lineage lymphomas. A20 is frequently inactivated by somatic mutations and/or deletions in mucosa-associated tissue lymphoma (18 out of 87; 21.8%) and Hodgkin's lymphoma of nodular sclerosis histology (5 out of 15; 33.3%), and, to a lesser extent, in other B-lineage lymphomas. When re-expressed in a lymphoma-derived cell line with no functional *A20* alleles, wild-type A20, but not mutant A20, resulted in suppression of cell growth and induction of apoptosis, accompanied by downregulation of NF-κB activation. The A20-deficient cells stably generated tumours in immunodeficient mice, whereas the tumorigenicity was effectively suppressed by re-expression of A20. In A20-deficient cells, suppression of both cell growth and NF-κB activity due to re-expression of A20 depended, at least partly, on cell-surface-receptor signalling, including the tumour-necrosis factor receptor. Considering the physiological function of A20 in the negative modulation of NF-κB activation induced by multiple upstream stimuli, our findings indicate that uncontrolled signalling of NF-κB caused by loss of A20 function is involved in the pathogenesis of subsets of B-lineage lymphomas.

Malignant lymphomas of B-cell lineages are mature lymphoid neoplasms that arise from various lymphoid tissues[10,11]. To obtain a comprehensive registry of genetic lesions in B-lineage lymphomas, we performed a single nucleotide polymorphism (SNP) array analysis of 238 primary B-cell lymphoma specimens of different histologies, including 64 samples of diffuse large B-cell lymphomas (DLBCLs), 52 follicular lymphomas, 35 mantle cell lymphomas (MCLs), and 87 mucosa-associated tissue (MALT) lymphomas (Supplementary Table 1). Three Hodgkin's-lymphoma-derived cell lines were also analysed. Interrogating more than 250,000 SNP sites, this platform permitted the identification of copy number changes at an average resolution of less than 12 kilobases (kb). The use of large numbers of SNP-specific probes is a unique feature of this platform, and combined with the CNAG/AsCNAR software, enabled accurate determination of 'allele-specific' copy numbers, and thus allowed for sensitive detection of loss of heterozygosity (LOH) even without apparent copy-number reduction, in the presence of up to 70–80% normal cell contamination[12,13].

Lymphoma genomes underwent a wide range of genetic changes, including numerical chromosomal abnormalities and segmental gains and losses of chromosomal material (Supplementary Fig. 1), as well as copy-number-neutral LOH, or uniparental disomy (Supplementary Fig. 2). Each histology type had a unique genomic signature, indicating a distinctive underlying molecular pathogenesis for different histology types (Fig. 1a and Supplementary Fig. 3). On the basis of the genomic signatures, the initial pathological diagnosis of MCL was re-evaluated and corrected to DLBCL in two cases. Although most copy number changes involved large chromosomal segments, a number of regions showed focal gains and deletions, accelerating identification of their candidate gene targets. After excluding known copy number variations, we identified 46 loci showing focal gains (19 loci) or deletions (27 loci) (Supplementary Tables 2 and 3 and Supplementary Fig. 4).

Genetic lesions on the NF-κB pathway were common in B-cell lymphomas and found in approximately 40% of the cases (Supplementary Table 1), underpinning the importance of aberrant NF-κB activation in lymphomagenesis[11,14] in a genome-wide fashion. They included focal gain/amplification at the *REL* locus (16.4%) (Fig. 1b) and *TRAF6* locus (5.9%), as well as focal deletions at the *PTEN* locus (5.5%) (Supplementary Figs 1 and 4). However, the most striking finding was the common deletion at 6q23.3 involving a 143-kb segment. It exclusively contained the *A20* gene (also called *TNFAIP3*), a negative regulator of NF-κB activation[3–7,15] (Fig. 1b), which was previously reported as a candidate target of 6q23 deletions in ocular lymphoma[16]. LOH involving the *A20* locus was found in 50 cases, of which 12 showed homozygous deletions as determined by the loss of both alleles in an allele-specific copy number analysis (Fig. 1b, Table 1 and Supplementary Table 4). On the basis of this finding, we searched for possible tumour-specific mutations of *A20* by genomic DNA sequencing of entire coding exons of the gene in the same series of lymphoma samples (Supplementary Fig. 5). Because two out of the three Hodgkin's-lymphoma-derived cell lines had biallelic *A20* deletions/mutations (Supplementary Fig. 6), 24 primary samples from Hodgkin's lymphoma were also analysed for mutations, where

[1]Cancer Genomics Project, Department of [2]Pediatrics, [3]Cell Therapy and Transplantation Medicine, and [4]Hematology and Oncology, Graduate School of Medicine, University of Tokyo, 7-3-1 Hongo, Bunkyo-ku, Tokyo 113-8655, Japan. [5]Core Research for Evolutional Science and Technology, Japan Science and Technology Agency, 4-1-8, Honcho, Kawaguchi-shi, Saitama 332-0012, Japan. [6]Department of Pediatrics, Graduate School of Medicine, Kyoto University, 54 Kawahara-cho, Shogoin, Sakyo-ku, Kyoto 606-8507, Japan. [7]Department of Pathology, Okayama University Graduate School of Medicine, Dentistry and Pharmaceutical Sciences, 2-5-1 Shikata-cho, Kita-ku, Okayama 700-8558, Japan. [8]Division of Pathology, The Cancer Institute of Japanese Foundation for Cancer Research, Japan, 3-10-6 Ariake, Koto-ku, Tokyo 135-8550, Japan. [9]Hematology Division, Hospital, and [10]Early Oncogenesis Research Project, Research Institute, National Cancer Center, 5-1-1 Tsukiji, Chuo-ku, Tokyo 104-0045, Japan. [11]Division of Immunology, Aichi Cancer Center Research Institute, 1-1 Kanokoden, Chikusa-ku, Nagoya 464-8681, Japan. [12]Gunma Children's Medical Center, 779 Shimohakoda, Hokkitsu-machi, Shibukawa 377-8577, Japan. [13]Division of Hematology, Internal Medicine, Showa University Fujigaoka Hospital, 1-30, Fujigaoka, Aoba-ku, Yokohama-shi, Kanagawa 227-8501, Japan. [14]Department of Pathology, Teikyo University School of Medicine, 2-11-1 Kaga, Itabashi-ku, Tokyo 173-8605, Japan.

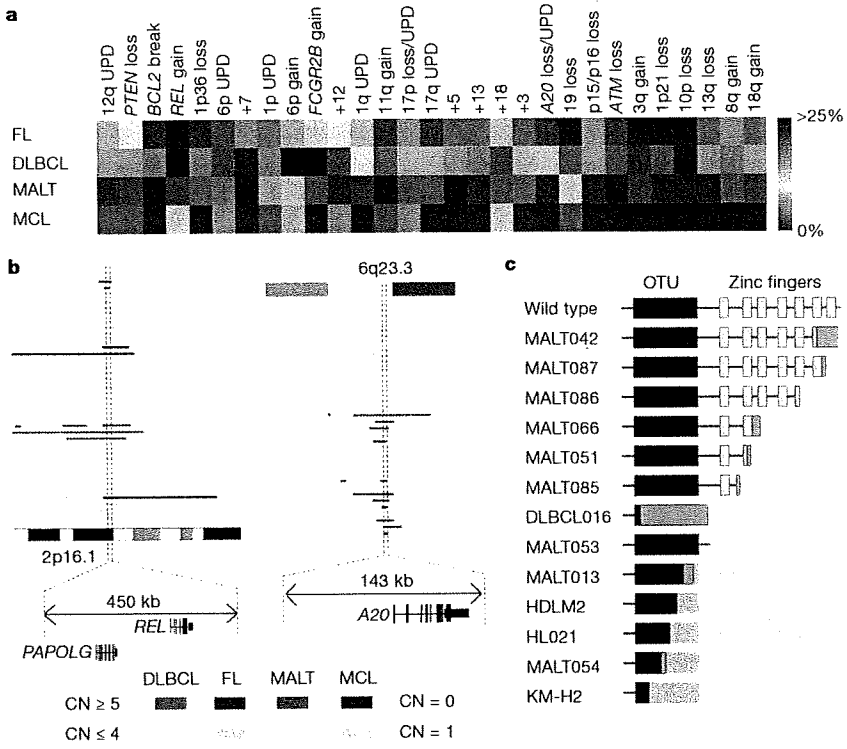

Figure 1 | Genomic signatures of different B-cell lymphomas and common genetic lesions at 2p16-15 and 6q23.3 involving NF-κB pathway genes. **a**, Twenty-nine genetic lesions were found in more than 10% in at least one histology and used for clustering four distinct histology types of B-lineage lymphomas. The frequency of each genetic lesion in each histology type is colour-coded. FL, follicular lymphoma; UPD, uniparental disomy. **b**, Recurrent genetic changes are depicted based on CNAG output of the SNP array analysis of 238 B-lineage lymphoma samples, which include gains at the *REL* locus on 2p16-15 (left panel) and the *A20* locus on 6q23.3 (right panel). Regions showing copy number gain or loss are indicated by horizontal lines. Four histology types are indicated by different colours, where high-grade amplifications and homozygous deletions are shown by darker shades to discriminate from simple gains (copy number ≤4) and losses (copy number = 1) (lighter shades). **c**, Point mutations and small nucleotide insertions and deletions in the *A20* (*TNFAIP3*) gene caused premature truncation of A20 in most cases. Altered amino acids caused by frame shifts are indicated by green bars.

genomic DNA was extracted from 150 microdissected CD30-positive tumour cells (Reed–Sternberg cells) for each sample. *A20* mutations were found in 18 out of 265 lymphoma samples (6.8%) (Table 1), among which 13 mutations, including nonsense mutations (3 cases), frame-shift insertions/deletions (9 cases), and a splicing donor site mutation (1 case) were thought to result in premature termination of translation (Fig. 1c). Four missense mutations and one intronic mutation were identified in five microdissected Hodgkin's lymphoma samples. They were not found in the surrounding normal tissues, and thus, were considered as tumour-specific somatic changes.

In total, biallelic *A20* lesions were found in 31 out of 265 lymphoma samples including 3 Hodgkin's lymphoma cell lines. Quantitative analysis of SNP array data suggested that these *A20* lesions were present in the major tumour fraction within the samples (Supplementary Fig. 7). Inactivation of *A20* was most frequent in MALT lymphoma (18 out of 87) and Hodgkin's lymphoma (7 out of 27), although it was also found in DLBCL (5 out of 64) and follicular lymphoma (1 out of 52) at lower frequencies. In MALT lymphoma, biallelic *A20* lesions were confirmed in 18 out of 24 cases (75.0%) with LOH involving the 6q23.3 segment (Supplementary Fig. 8). Considering the limitation in detecting very small homozygous deletions, *A20* was thought to be the target of 6q23 LOH in MALT lymphoma. On the other hand, the 6q23 LOHs in other histology types tended to be extended into more centromeric regions and less frequently accompanied biallelic *A20* lesions (Supplementary Fig. 8 and Supplementary Table 4), indicating that they might be more heterogeneous with regard to their gene targets. We were unable to analyse Hodgkin's lymphoma samples using SNP arrays owing to insufficient genomic DNA obtained from microdissected samples, and were likely to underestimate the frequency of *A20* inactivation in Hodgkin's lymphoma because we might fail to detect a substantial proportion of cases with homozygous deletions, which explained 50% (12 out of 24) of *A20* inactivation in other histology types. *A20* mutations in Hodgkin's lymphoma were exclusively found in nodular sclerosis classical Hodgkin's lymphoma (5 out of 15) but not in other histology types (0 out of 9), although the possible association requires further confirmation in additional cases.

A20 is a key regulator of NF-κB signalling, negatively modulating NF-κB activation through a wide variety of cell surface receptors and viral proteins, including tumour-necrosis factor (TNF) receptors, toll-like receptors, CD40, as well as Epstein–Barr-virus-associated LMP1 protein[2,5,17,18]. To investigate the role of A20 inactivation in lymphomagenesis, we re-expressed wild-type A20 under a *Tet*-inducible promoter in a lymphoma-derived cell line (KM-H2) that had no functional *A20* alleles (Supplementary Fig. 6), and examined the effect of A20 re-expression on cell proliferation, survival and downstream NF-κB signalling pathways. As shown in Fig. 2a–c and Supplementary Fig. 9, re-expression of wild-type A20 resulted in the suppression of cell proliferation and enhanced apoptosis, and in the concomitant accumulation of IκBβ and IκBε, and downregulation of NF-κB activity. In contrast, re-expression of two lymphoma-derived A20 mutants, $A20^{532Stop}$ or $A20^{750Stop}$, failed to show growth suppression, induction of apoptosis, accumulation of IκBβ and IκBε or downregulation of

Table 1 | Inactivation of A20 in B-lineage lymphomas

Histology	Tissue	Sample	Allele	Uniparental disomy	Exon	Mutation	Biallelic inactivation
DLBCL							5 out of 64 (7.8%)
	Lymph node	DLBCL008	−/−	No	–	–	
	Lymph node	DLBCL016	+/−	No	Ex2	329insA	
	Lymph node	DLBCL022	−/−	No	–	–	
	Lymph node	DLBCL028	−/−	Yes	–	–	
	Lymph node	MCL008*	−/−	Yes	–	–	
Follicular lymphoma							1 out of 52 (1.9%)
	Lymph node	FL024	−/−	No	–	–	
MCL							0 out of 35 (0%)
MALT							18 out of 87 (21.8%)
Stomach							3 out of 23 (13.0%)
	Gastric mucosa	MALT013	+/+	Yes	Ex5	705insG	
	Gastric mucosa	MALT014	+/+	Yes	Ex3	Ex3 donor site>A	
	Gastric mucosa	MALT036	+/−	No	Ex7	delintron6-Ex7†	
Eye							13 out of 43 (30.2%)
	Ocular adnexa	MALT008	−/−	No	–	–	
	Ocular adnexa	MALT017	−/−	No	–	–	
	Ocular adnexa	MALT051	+/−	No	Ex7	1943delTG	
	Ocular adnexa	MALT053	+/+	Yes	Ex6	1016G>A(stop)	
	Ocular adnexa	MALT054	+/−	No	Ex3	502delTC	
	Ocular adnexa	MALT055	−/−	No	–	–	
	Ocular adnexa	MALT066	+/−	No	Ex7	1581insA	
	Ocular adnexa	MALT067	−/−	No	–	–	
	Ocular adnexa	MALT082	−/−	Yes	–	–	
	Ocular adnexa	MALT084	−/−	Yes	–	–	
	Ocular adnexa	MALT085	+/+	Yes	Ex7	1435insG	
	Ocular adnexa	MALT086	+/+	Yes	Ex6	878C>T(stop)	
	Ocular adnexa	MALT087	+/+	Yes	Ex9	2304delGG	
Lung							2 out of 12 (16.7%)
	Lung	MALT042	−/−	No	–	–	
	Lung	MALT047	+/+	Yes	Ex9	2281insT	
Other‡							0 out of 9 (0%)
Hodgkin's lymphoma							7 out of 27 (26.0%)
NSHL	Lymph node	HL10	ND	ND	Ex7	1777G>A(V571I)	
NSHL	Lymph node	HL12	ND	ND	Ex7	1156A>G(R364G)	
NSHL	Lymph node	HL21	ND	ND	Ex4	569G>A(stop)	
NSHL	Lymph node	HL24	ND	ND	Ex3	1487C>A(T474N)	
NSHL	Lymph node	HL23	ND	ND	–	Intron 3§	
	Cell line	KM-H2	−/−	No	–		
	Cell line	HDLM2	+/−	No	Ex4	616ins29bp‖	
Total							31 out of 265 (11.7%)

DLBCL, diffuse large B-cell lymphoma; MALT, MALT lymphoma; MCL, mantle cell lymphoma; ND, not determined because SNP array analysis was not performed; NSHL, nodular sclerosis classical Hodgkin's lymphoma.
* Diagnosis was changed based on the genomic data, which was confirmed by re-examination of pathology.
† Deletion including the boundary of intron 6 and exon 7 (see also Supplementary Fig. 5b).
‡ Including 1 parotid gland, 1 salivary gland, 2 colon and 5 thyroid cases.
§ Insertion of CTC at −19 bases from the beginning of exon 3.
‖ Insertion of TGGCTTCCACAGACACACCCATGGCCCGA.

NF-κB activity (Fig. 2a–c), indicating that these were actually loss-of-function mutations. To investigate the role of A20 inactivation in lymphomagenesis *in vivo*, *A20*- and mock-transduced KM-H2 cells were transplanted in NOD/SCID/γ_c^{null} (NOG) mice[19], and their tumour formation status was examined for 5 weeks with or without induction of wild-type A20 by tetracycline administration. As shown in Fig. 2d, mock-transduced cells developed tumours at the injected sites, whereas the *Tet*-inducible *A20*-transduced cells generated tumours only in the absence of A20 induction (Supplementary Table 5), further supporting the tumour suppressor role of A20 in lymphoma development.

Given the mode of negative regulation of NF-κB signalling, we next investigated the origins of NF-κB activity that was deregulated by A20 loss in KM-H2 cells. The conditioned medium prepared from a 48-h serum-free KM-H2 culture had increased NF-κB upregulatory activity compared with fresh serum-free medium, which was inhibited by re-expression of A20 (Fig. 3a). KM-H2 cells secreted two known ligands for TNF receptor—TNF-α and lymphotoxin-α (Supplementary Fig. 10)[20]—and adding neutralizing antibodies against these cytokines into cultures significantly suppressed their cell growth and NF-κB activity without affecting the levels of their overall suppression after A20 induction (Fig. 3b, d). In addition, recombinant TNF-α and/or lymphotoxin-α added to fresh serum-free medium promoted cell growth and NF-κB activation in KM-H2 culture, which were again suppressed by re-expression of A20 (Fig. 3c, e). Although our data in Fig. 3 also show the presence of factors other than TNF-α and lymphotoxin-α in the KM-H2-conditioned medium—as well as some intrinsic pathways in the cell (Fig. 3a)—that were responsible for the A20-dependent NF-κB activation, these results indicate that both cell growth and NF-κB activity that were upregulated by A20 inactivation depend at least partly on the upstream stimuli that evoked the NF-κB-activating signals.

Aberrant activation of the NF-κB pathway is a hallmark of several subtypes of B-lineage lymphomas, including Hodgkin's lymphoma, MALT lymphoma, and a subset of DLBCL, as well as other lymphoid neoplasms[11,14], where a number of genetic alterations of NF-κB signalling pathway genes[21–25], as well as some viral proteins[26,27], have been implicated in the aberrant activation of the NF-κB pathway[14]. Thus, frequent inactivation of A20 in Hodgkin's lymphoma and MALT and other lymphomas provides a novel insight into the molecular pathogenesis of these subtypes of B-lineage lymphomas through deregulated NF-κB activation. Because A20 provides a

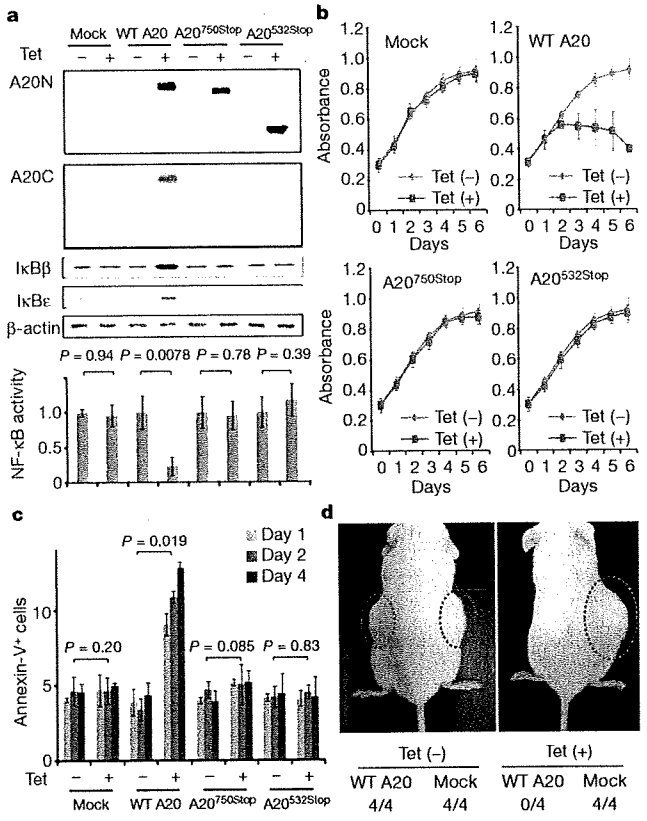

Figure 2 | Effects of wild-type and mutant A20 re-expressed in a lymphoma cell line that lacks the normal *A20* gene. a, Western blot analyses of wild-type (WT) and mutant ($A20^{532Stop}$ and $A20^{750Stop}$) A20, as well as IκBβ and IκBε, in KM-H2 cells, in the presence or absence of tetracycline treatment (top panels). A20N and A20C are polyclonal antisera raised against N-terminal and C-terminal A20 peptides, respectively. β-actin blots are provided as a control. NF-κB activities are expressed as mean absorbance ± s.d. ($n = 6$) in luciferase assays (bottom panel). **b,** Proliferation of KM-H2 cells stably transduced with plasmids for mock and *Tet*-inducible wild-type A20, $A20^{532Stop}$ and $A20^{750Stop}$ was measured using a cell counting kit in the presence (red lines) or absence (blue lines) of tetracycline. Mean absorbance ± s.d. ($n = 5$) is plotted. **c,** The fractions of Annexin-V-positive KM-H2 cells transduced with various *Tet*-inducible A20 constructs were measured by flow cytometry after tetracycline treatment and the mean values (±s.d., $n = 3$) are plotted. **d,** *In vivo* tumorigenicity was assayed by inoculating 7×10^6 KM-H2 cells transduced with mock or *Tet*-inducible wild-type A20 in NOG mice, with (right panel) or without (left panel) tetracycline administration.

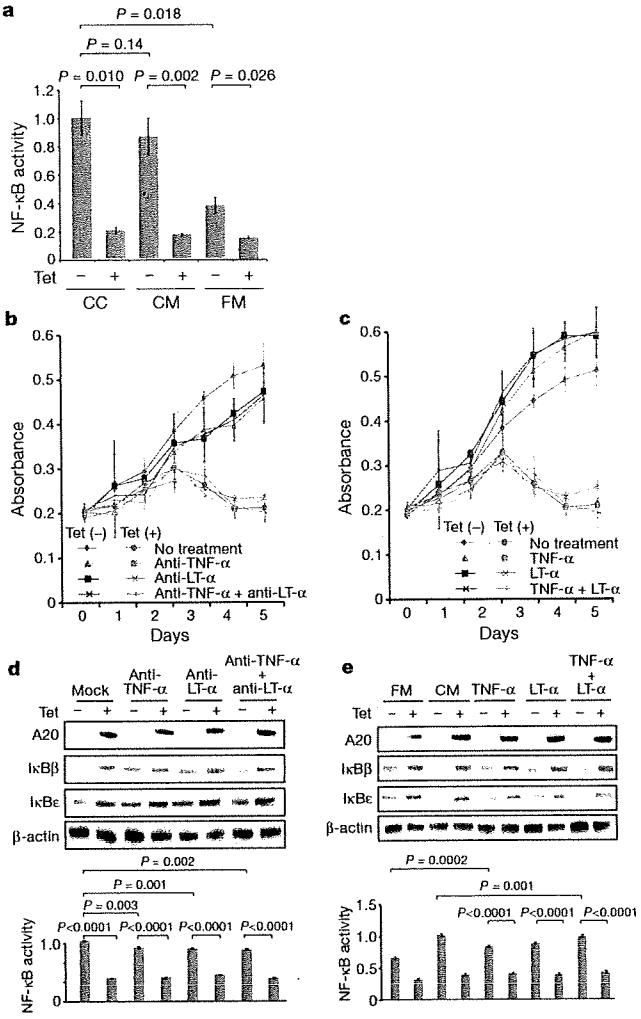

Figure 3 | Tumour suppressor role of A20 under external stimuli. a, NF-κB activity in KM-H2 cells was measured 30 min after cells were inoculated into fresh medium (FM) or KM-H2-conditioned medium (CM) obtained from the 48-h culture of KM-H2, and was compared with the activity after 48 h continuous culture of KM-H2 (CC). A20 was induced 12 h before inoculation in Tet (+) groups. **b, c,** Effects of neutralizing antibodies against TNF-α and lymphotoxin-α (LTα) (**b**) and of recombinant TNF-α and LT-α added to the culture (**c**) on cell growth were evaluated in the presence (Tet (+)) or absence (Tet (−)) of A20 induction. Cell numbers were measured using a cell counting kit and are plotted as their mean absorbance ± s.d. ($n = 6$). **d, e,** Effects of the neutralizing antibodies (**d**) and the recombinant cytokines added to the culture (**e**) on NF-κB activities and the levels of IκBβ and IκBε after 48 h culture with (Tet (+)) or without (Tet (−)) tetracycline treatment. NF-κB activities are expressed as mean absorbance ± s.d. ($n = 6$) in luciferase assays.

negative feedback mechanism in the regulation of NF-κB signalling pathways upon a variety of stimuli, aberrant activation of NF-κB will be a logical consequence of A20 inactivation. However, there is also the possibility that the aberrant NF-κB activity of A20-inactivated lymphoma cells is derived from upstream stimuli, which may be from the cellular environment. In this context, it is intriguing that MALT lymphoma usually arises at the site of chronic inflammation caused by infection or autoimmune disorders and may show spontaneous regression after eradication of infectious organisms[28]; furthermore, Hodgkin's lymphoma frequently shows deregulated cytokine production from Reed–Sternberg cells and/or surrounding reactive cells[29]. Detailed characterization of the NF-κB pathway regulated by A20 in both normal and neoplastic B lymphocytes will promote our understanding of the precise roles of A20 inactivation in the pathogenesis of these lymphoma types. Our finding underscores the importance of genome-wide approaches in the identification of genetic targets in human cancers.

METHODS SUMMARY

Genomic DNA from 238 patients with non-Hodgkin's lymphoma and three Hodgkin's-lymphoma-derived cell lines was analysed using GeneChip SNP genotyping microarrays (Affymetrix). This study was approved by the ethics boards of the University of Tokyo, National Cancer Institute Hospital, Okayama University, and the Cancer Institute of the Japanese Foundation of Cancer Research. After appropriate normalization of mean array intensities, signal ratios between tumours and anonymous normal references were calculated in an allele-specific manner, and allele-specific copy numbers were inferred from the observed signal ratios based on the hidden Markov model using CNAG/AsCNAR software (http://www.genome.umin.jp). *A20* mutations were examined by directly sequencing genomic DNA using a set of primers (Supplementary Table 6). Full-length cDNAs of wild-type and mutant *A20* were introduced into a

lentivirus vector, pLenti4/TO/V5-DEST (Invitrogen), with a *Tet*-inducible promoter. Viral stocks were prepared by transfecting the vector plasmids into 293FT cells (Invitrogen) using the calcium phosphate method and then infected to the KM-H2 cell line. Proliferation of KM-H2 cells was measured using a Cell Counting Kit (Dojindo). Western blot analyses and luciferase assays were performed as previously described. NF-κB activity was measured by luciferase assays in KM-H2 cells stably transduced with a reporter plasmid having an NF-κB response element, pGL4.32 (Promega). Apoptosis of KM-H2 upon A20 induction was evaluated by counting Annexin-V-positive cells by flow cytometry. For *in vivo* tumorigenicity assays, 7×10^6 KM-H2 cells were transduced with the *Tet*-inducible *A20* gene and those with a mock vector were inoculated on the contralateral sides in eight NOG mice[19] and examined for their tumour formation with ($n = 4$) or without ($n = 4$) tetracycline administration. Full copy number data of the 238 lymphoma samples will be accessible from the Gene Expression Omnibus (GEO, http://ncbi.nlm.nih.gov/geo/) with the accession number GSE12906.

Full Methods and any associated references are available in the online version of the paper at www.nature.com/nature.

Received 17 September 2008; accepted 3 March 2009.
Published online 3 May 2009.

1. Dixit, V. M. *et al.* Tumor necrosis factor-α induction of novel gene products in human endothelial cells including a macrophage-specific chemotaxin. *J. Biol. Chem.* 265, 2973–2978 (1990).
2. Song, H. Y., Rothe, M. & Goeddel, D. V. The tumor necrosis factor-inducible zinc finger protein A20 interacts with TRAF1/TRAF2 and inhibits NF-κB activation. *Proc. Natl Acad. Sci. USA* 93, 6721–6725 (1996).
3. Lee, E. G. *et al.* Failure to regulate TNF-induced NF-κB and cell death responses in A20-deficient mice. *Science* 289, 2350–2354 (2000).
4. Boone, D. L. *et al.* The ubiquitin-modifying enzyme A20 is required for termination of Toll-like receptor responses. *Nature Immunol.* 5, 1052–1060 (2004).
5. Wang, Y. Y., Li, L., Han, K. J., Zhai, Z. & Shu, H. B. A20 is a potent inhibitor of TLR3- and Sendai virus-induced activation of NF-κB and ISRE and IFN-β promoter. *FEBS Lett.* 576, 86–90 (2004).
6. Wertz, I. E. *et al.* De-ubiquitination and ubiquitin ligase domains of A20 downregulate NF-κB signalling. *Nature* 430, 694–699 (2004).
7. Heyninck, K. & Beyaert, R. A20 inhibits NF-κB activation by dual ubiquitin-editing functions. *Trends Biochem. Sci.* 30, 1–4 (2005).
8. Graham, R. R. *et al.* Genetic variants near *TNFAIP3* on 6q23 are associated with systemic lupus erythematosus. *Nature Genet.* 40, 1059–1061 (2008).
9. Musone, S. L. *et al.* Multiple polymorphisms in the *TNFAIP3* region are independently associated with systemic lupus erythematosus. *Nature Genet.* 40, 1062–1064 (2008).
10. Jaffe, E. S., Harris, N. L., Stein, H. & Vardiman, J. W. *World Health Organization Classification of Tumours. Pathology and Genetics of Tumours of Hematopoietic and Lymphoid Tissues* (IARC Press, 2001).
11. Klein, U. & Dalla-Favera, R. Germinal centres: role in B-cell physiology and malignancy. *Nature Rev. Immunol.* 8, 22–33 (2008).
12. Nannya, Y. *et al.* A robust algorithm for copy number detection using high-density oligonucleotide single nucleotide polymorphism genotyping arrays. *Cancer Res.* 65, 6071–6079 (2005).
13. Yamamoto, G. *et al.* Highly sensitive method for genomewide detection of allelic composition in nonpaired, primary tumor specimens by use of affymetrix single-nucleotide-polymorphism genotyping microarrays. *Am. J. Hum. Genet.* 81, 114–126 (2007).
14. Jost, P. J. & Ruland, J. Aberrant NF-κB signaling in lymphoma: mechanisms, consequences, and therapeutic implications. *Blood* 109, 2700–2707 (2007).
15. Durkop, H., Hirsch, B., Hahn, C., Foss, H. D. & Stein, H. Differential expression and function of A20 and TRAF1 in Hodgkin lymphoma and anaplastic large cell lymphoma and their induction by CD30 stimulation. *J. Pathol.* 200, 229–239 (2003).
16. Honma, K. *et al. TNFAIP3* is the target gene of chromosome band 6q23.3-q24.1 loss in ocular adnexal marginal zone B cell lymphoma. *Genes Chromosom. Cancer* 47, 1–7 (2008).
17. Sarma, V. *et al.* Activation of the B-cell surface receptor CD40 induces A20, a novel zinc finger protein that inhibits apoptosis. *J. Biol. Chem.* 270, 12343–12346 (1995).
18. Fries, K. L., Miller, W. E. & Raab-Traub, N. The A20 protein interacts with the Epstein-Barr virus latent membrane protein 1 (LMP1) and alters the LMP1/TRAF1/TRADD complex. *Virology* 264, 159–166 (1999).
19. Hiramatsu, H. *et al.* Complete reconstitution of human lymphocytes from cord blood $CD34^+$ cells using the NOD/SCID/γ^{null} mice model. *Blood* 102, 873–880 (2003).
20. Hsu, P. L. & Hsu, S. M. Production of tumor necrosis factor-α and lymphotoxin by cells of Hodgkin's neoplastic cell lines HDLM-1 and KM-H2. *Am. J. Pathol.* 135, 735–745 (1989).
21. Dierlamm, J. *et al.* The apoptosis inhibitor gene *API2* and a novel 18q gene, *MLT*, are recurrently rearranged in the t(11;18)(q21;q21) associated with mucosa-associated lymphoid tissue lymphomas. *Blood* 93, 3601–3609 (1999).
22. Willis, T. G. *et al.* Bcl10 is involved in t(1;14)(p22;q32) of MALT B cell lymphoma and mutated in multiple tumor types. *Cell* 96, 35–45 (1999).
23. Joos, S. *et al.* Classical Hodgkin lymphoma is characterized by recurrent copy number gains of the short arm of chromosome 2. *Blood* 99, 1381–1387 (2002).
24. Martin-Subero, J. I. *et al.* Recurrent involvement of the *REL* and *BCL11A* loci in classical Hodgkin lymphoma. *Blood* 99, 1474–1477 (2002).
25. Lenz, G. *et al.* Oncogenic *CARD11* mutations in human diffuse large B cell lymphoma. *Science* 319, 1676–1679 (2008).
26. Deacon, E. M. *et al.* Epstein-Barr virus and Hodgkin's disease: transcriptional analysis of virus latency in the malignant cells. *J. Exp. Med.* 177, 339–349 (1993).
27. Yin, M. J. *et al.* HTLV-I Tax protein binds to MEKK1 to stimulate IκB kinase activity and NF-κB activation. *Cell* 93, 875–884 (1998).
28. Isaacson, P. G. & Du, M. Q. MALT lymphoma: from morphology to molecules. *Nature Rev. Cancer* 4, 644–653 (2004).
29. Skinnider, B. F. & Mak, T. W. The role of cytokines in classical Hodgkin lymphoma. *Blood* 99, 4283–4297 (2002).

Supplementary Information is linked to the online version of the paper at www.nature.com/nature.

Acknowledgements This work was supported by the Core Research for Evolutional Science and Technology, Japan Science and Technology Agency, by the 21st century centre of excellence program 'Study on diseases caused by environment/genome interactions', and by Grant-in-Aids from the Ministry of Education, Culture, Sports, Science and Technology of Japan and from the Ministry of Health, Labor and Welfare of Japan for the 3rd-term Comprehensive 10-year Strategy for Cancer Control. We also thank Y. Ogino, E. Matsui and M. Matsumura for their technical assistance.

Author Contributions M.Ka., K.N. and M.S. performed microarray experiments and subsequent data analyses. M.Ka., Y.C., K.Ta., J.T., J.N., M.I., A.T. and Y.K. performed mutation analysis of *A20*. M.Ka., S.Mu., M.S., Y.C. and Y.Ak. conducted functional assays of mutant A20. Y.S., K.Ta., Y.As., H.M., M.Ku., S.Mo., S.C., Y.K., K.To. and Y.I. prepared tumour specimens. I.K., K.O., A.N., H.N. and T.N. conducted *in vivo* tumorigenicity experiments in NOG/SCID mice. T.I., Y.H., T.Y., Y.K. and S.O. designed overall studies, and S.O. wrote the manuscript. All authors discussed the results and commented on the manuscript.

Author Information The copy number data as well as the raw microarray data will be accessible from the GEO (http://ncbi.nlm.nih.gov/geo/) with the accession number GSE12906. Reprints and permissions information is available at www.nature.com/reprints. Correspondence and requests for materials should be addressed to S.O. (sogawa-tky@umin.ac.jp) or Y.K. (ykkobaya@ncc.go.jp).

METHODS

Specimens. Primary tumour specimens were obtained from patients who were diagnosed with DLBCL, follicular lymphoma, MCL, MALT lymphoma, or classical Hodgkin's lymphoma. In total, 238 primary lymphoma specimens listed in Supplementary Table 1 were subjected to SNP array analysis. Three Hodgkin's-lymphoma-derived cell lines (KM-H2, HDLM2, L540) were obtained from Hayashibara Biochemical Laboratories, Inc., Fujisaki Cell Center and were also analysed by SNP array analysis.

Microarray analysis. High-molecular-mass DNA was isolated from tumour specimens and subjected to SNP array analysis using GeneChip Mapping 50K and/or 250K arrays (Affymetrix). The scanned array images were processed with Gene Chip Operation software (GCOS), followed by SNP calls using GTYPE. Genome-wide copy number measurements and LOH detection were performed using CNAG/AsCNAR software[12,13].

Mutation analysis. Mutations in the *A20* gene were examined in 265 samples of B-lineage lymphoma, including 62 DLBCLs, 52 follicular lymphomas, 87 MALTs, 37 MCLs and 3 Hodgkin's-lymphoma-derived cell lines and 24 primary Hodgkin's lymphoma samples, by direct sequencing using an ABI PRISM 3130xl Genetic Analyser (Applied Biosystems). To analyse primary Hodgkin's lymphoma samples in which CD30-positive tumour cells (Reed–Sternberg cells) account for only a fraction of the specimen, 150 Reed–Sternberg cells were collected for each 10 μm slice of a formalin-fixed block immunostained for CD30 by laser-capture microdissection (ASLMD6000, Leica), followed by genomic DNA extraction using QIAamp DNA Micro kit (Qiagen). The primer sets used in this study are listed in Supplementary Table 6.

Functional analysis of wild-type and mutant A20. Full-length cDNA for wild-type *A20* was isolated from total RNA extracted from an acute myeloid leukaemia-derived cell line, CTS, and subcloned into a lentivirus vector (pLenti4/TO/V5-DEST, Invitrogen). cDNAs for mutant A20 were generated by PCR amplification using mutagenic primers (Supplementary Table 6), and introduced into the same lentivirus vector. Forty-eight hours after transfection of each plasmid into 293FT cells using the calcium phosphate method, lentivirus stocks were obtained from ultrafiltration using Amicon Ultra (Millipore), and used to infect KM-H2 cells to generate stable transfectants of mock, wild-type and mutant A20. Each KM-H2 derivative cell line was further transduced stably with a reporter plasmid (pGL4.32, Promega) containing a luciferase gene under an NF-κB-responsive element by electroporation using Nucleofector reagents (Amaxa).

Assays for cell proliferation and NF-κB activity. Proliferation of the KM-H2 derivative cell lines was assayed in triplicate using a Cell Counting Kit (Dojindo). The mean absorption of five independent assays was plotted with s.d. for each derivative line. Two independent KM-H2-derived cell lines were used for each experiment. The NF-κB activity in KM-H2 derivatives for A20 mutants was evaluated by luciferase assays using a PiccaGene Luciferase Assay Kit (TOYO B-Net Co.). Each assay was performed in triplicate and the mean absorption of five independent experiments was plotted with s.d.

Western blot analyses. Polyclonal anti-sera against N-terminal (anti-A20N) and C-terminal (anti-A20C) A20 peptides were generated by immunizing rabbits with these peptides (LSNMRKAVKIRERTPEDIC for anti-A20N and CFQFKQMYG for anti-A20C, respectively). Total cell lysates from KM-H2 cells were separated on 7.5% polyacrylamide gel and subjected to western blot analysis using antibodies to A20 (anti-A20N and anti-A20C), IκBα (sc-847), IκBβ (sc-945), IκBγ (sc-7155) and actin (sc-8432) (Santa Cruz Biotechnology).

Functional analyses of wild-type and mutant A20. Each KM-H2 derivative cell line stably transduced with various *Tet*-inducible A20 constructs was cultured in serum-free medium in the presence or absence of A20 induction using 1 μg ml^{-1} of tetracycline, and cell number was counted every day. 1×10^6 cells of each KM-H2 derivative cell line were analysed for their intracellular levels of IκBβ and IκBε and for NF-κB activities by western blot analyses and luciferase assays, respectively, 12 h after the beginning of cell culture. Effects of human recombinant TNF-α and lymphotoxin-α (210-TA and 211-TB, respectively, R&D Systems) on the NF-κB pathway and cell proliferation were evaluated by adding both cytokines into 10 ml of serum-free cell culture at a concentration of 200 pg ml^{-1}. For cell proliferation assays, culture medium was half replaced every 12 h to minimize the side-effects of autocrine cytokines. Intracellular levels of IκBβ, IκBε and NF-κB were examined 12 h after the beginning of the cell culture. To evaluate the effect of neutralizing TNF-α and lymphotoxin-α, 1×10^6 of KM-H2 cells transduced with both *Tet*-inducible A20 and the NF-κB-luciferase reporter were pre-cultured in serum-free media for 36 h, and thereafter neutralizing antibodies against TNF-α (MAB210, R&D Systems) and/or lymphotoxin-α (AF-211-NA, R&D Systems) were added to the media at a concentration of 200 pg ml^{-1}. After the extended culture during 12 h with or without 1 μg ml^{-1} tetracycline, the intracellular levels of IκBβ and IκBε and NF-κB activities were examined by western blot analysis and luciferase assays, respectively. To examine the effects of A20 re-expression on apoptosis, 1×10^6 KM-H2 cells were cultured for 4 days in 10 ml medium with or without *Tet* induction. After staining with phycoerythrin-conjugated anti-Annexin-V (ID556422, Becton Dickinson), Annexin-V-positive cells were counted by flow cytometry at the indicated times.

***In vivo* tumorigenicity assays.** KM-H2 cells transduced with a mock or *Tet*-inducible wild-type *A20* gene were inoculated into NOG mice and their tumorigenicity was examined for 5 weeks with or without tetracycline administration. Injections of 7×10^6 cells of each KM-H2 cell line were administered to two opposite sites in four mice. Tetracycline was administered in drinking water at a concentration of 200 μg ml^{-1}.

ELISA. Concentrations of TNF-α, lymphotoxin-α, IL-1, IL-2, IL-4, IL-6, IL-12, IL-18 and TGF-β in the culture medium were measured after 48 h using ELISA. For those cytokines detectable after 48-h culture (TNFα, LTα, and IL-6), their time course was examined further using the Quantikine ELISA kit (R&D Systems).

Statistical analysis. Significance of the difference in NF-κB activity between two given groups was evaluated using a paired *t*-test, in which the data from each independent luciferase assay were paired to calculate test statistics. To evaluate the effect of A20 re-expression in KM-H2 cells on apoptosis, the difference in the fractions of Annexin-V-positive cells between Tet (+) and Tet (−) groups was also tested by a paired *t*-test for assays, in which the data from the assays performed on the same day were paired.

nature

Vol 460|13 August 2009|doi:10.1038/nature08240

LETTERS

Gain-of-function of mutated *C-CBL* tumour suppressor in myeloid neoplasms

Masashi Sanada[1,5]*, Takahiro Suzuki[7]*, Lee-Yung Shih[8]*, Makoto Otsu[9], Motohiro Kato[1,2], Satoshi Yamazaki[6], Azusa Tamura[1], Hiroaki Honda[11], Mamiko Sakata-Yanagimoto[12], Keiki Kumano[3], Hideaki Oda[13], Tetsuya Yamagata[14], Junko Takita[1,2,3], Noriko Gotoh[10], Kumi Nakazaki[1,4], Norihiko Kawamata[15], Masafumi Onodera[16], Masaharu Nobuyoshi[7], Yasuhide Hayashi[17], Hiroshi Harada[18], Mineo Kurokawa[3,4], Shigeru Chiba[12], Hiraku Mori[18], Keiya Ozawa[7], Mitsuhiro Omine[18], Hisamaru Hirai[3,4], Hiromitsu Nakauchi[6,9], H. Phillip Koeffler[15] & Seishi Ogawa[1,5]

Acquired uniparental disomy (aUPD) is a common feature of cancer genomes, leading to loss of heterozygosity. aUPD is associated not only with loss-of-function mutations of tumour suppressor genes[1], but also with gain-of-function mutations of proto-oncogenes[2]. Here we show unique gain-of-function mutations of the *C-CBL* (also known as *CBL*) tumour suppressor that are tightly associated with aUPD of the 11q arm in myeloid neoplasms showing myeloproliferative features. The *C-CBL* proto-oncogene, a cellular homologue of *v-Cbl*, encodes an E3 ubiquitin ligase and negatively regulates signal transduction of tyrosine kinases[3–6]. Homozygous *C-CBL* mutations were found in most 11q-aUPD-positive myeloid malignancies. Although the *C-CBL* mutations were oncogenic in NIH3T3 cells, c-Cbl was shown to functionally and genetically act as a tumour suppressor. C-CBL mutants did not have E3 ubiquitin ligase activity, but inhibited that of wild-type C-CBL and CBL-B (also known as CBLB), leading to prolonged activation of tyrosine kinases after cytokine stimulation. *c-Cbl*$^{-/-}$ haematopoietic stem/progenitor cells (HSPCs) showed enhanced sensitivity to a variety of cytokines compared to *c-Cbl*$^{+/+}$ HSPCs, and transduction of *C-CBL* mutants into *c-Cbl*$^{-/-}$ HSPCs further augmented their sensitivities to a broader spectrum of cytokines, including stem-cell factor (SCF, also known as KITLG), thrombopoietin (TPO, also known as THPO), IL3 and FLT3 ligand (FLT3LG), indicating the presence of a gain-of-function that could not be attributed to a simple loss-of-function. The gain-of-function effects of C-CBL mutants on cytokine sensitivity of HSPCs largely disappeared in a *c-Cbl*$^{+/+}$ background or by co-transduction of wild-type *C-CBL*, which suggests the pathogenic importance of loss of wild-type *C-CBL* alleles found in most cases of *C-CBL*-mutated myeloid neoplasms. Our findings provide a new insight into a role of gain-of-function mutations of a tumour suppressor associated with aUPD in the pathogenesis of some myeloid cancer subsets.

Myelodysplastic syndromes (MDS) are heterogeneous groups of blood cancers originating from haematopoietic precursors. They are characterized by deregulated haematopoiesis showing a high propensity to acute myeloid leukaemia (AML)[7]. Some MDS cases have overlapping clinico-pathological features with myeloproliferative disorders, and are now classified into myelodysplasia/myeloproliferative neoplasms (MDS/MPN) by the World Health Organization (WHO) classification[8]. To obtain a comprehensive profile of allelic imbalances in these myeloid neoplasms, we performed allele-specific copy number analyses of bone marrow samples obtained from 222 patients with MDS, MDS/MPN, or other related myeloid neoplasms (Supplementary Tables 1 and 2) using high-density single nucleotide polymorphism (SNP) arrays combined with CNAG/AsCNAR software[9,10].

Genomic profiles of MDS and MDS/MPN showed characteristic unbalanced genetic changes, as reported in previous cytogenetic studies[11] (Supplementary Fig. 1a); however, they were detected more sensitively by SNP array analyses (Supplementary Table 3). aUPD was detected in 70 samples (31.5%) on the basis of the allele-specific copy number analyses, which substantially exceeded the detection rate obtained using a SNP call-based detection algorithm (20.7%) (Supplementary Figs 2 and 4, and Supplementary Tables 4 and 5). Long stretches of homozygous SNP calls caused by shared identical-by-descent alleles in parents were empirically predicted and excluded (Supplementary Fig. 3). aUPDs were more common in MDS/MPN than in MDS. They preferentially affected several chromosomal arms (1p, 1q, 4q, 7q, 11p, 11q, 14q, 17p and 21q) in distinct subsets of patients, and frequently associated with mutated oncogenes and tumour suppressor genes (Supplementary Figs 1b and 5). Among these, the most common aUPDs were those involving 11q ($n = 17$), which defined a unique subset of myeloid neoplasms that were clinically characterized by frequent diagnosis of chronic myelomonocytic leukaemia (CMML) with normal karyotypes (13 cases) (Fig. 1a and Supplementary Table 6). We identified a minimum overlapping aUPD segment of approximately 1.4 megabases (Mb) in 11q, which contained a mutated *C-CBL* proto-oncogene (Fig. 1b).

[1]Cancer Genomics Project, [2]Department of Pediatrics, [3]Cell Therapy and Transplantation Medicine, and [4]Hematology and Oncology, Graduate School of Medicine, The University of Tokyo, 7-3-1 Hongo, Bunkyo-ku, Tokyo 113-8655, Japan. [5]Core Research for Evolutional Science and Technology, [6]Exploratory Research for Advanced Technology, Japan Science and Technology Agency, 4-1-8 Honcho, Kawaguchi-shi, Saitama 332-0012, Japan. [7]Division of Hematology, Department of Medicine, Jichi Medical University, 3311-1 Yakushiji, Shimotsuke-shi, Tochigi 329-0498, Japan. [8]Division of Hematology-Oncology, Department of Internal Medicine, Chang Gung Memorial Hospital, Chang Gung University, 199 Tung Hwa North Road, Taipei 105, Taiwan. [9]Division of Stem Cell Therapy, Center for Stem Cell and Regenerative Medicine, [10]Division of Systems Biomedical Technology, Institute of Medical Science, The University of Tokyo, 4-6-1 Shirokanedai, Minato-ku, Tokyo 108-8639, Japan. [11]Department of Developmental Biology, Research Institute of Radiation Biology and Medicine, Hiroshima University, 1-2-3 Kasumi, Minami-ku, Hiroshima 734-8553, Japan. [12]Department of Clinical and Experimental Hematology, Institute of Clinical Medicine, University of Tsukuba, 1-1-1 Tennodai, Tukuba-shi, Ibaraki, 305-8571, Japan. [13]Department of Pathology, Tokyo Women's Medical University, 8-1 Kawada-cho, Shinjuku-ku, Tokyo 162-8666, Japan. [14]Department of Hematology, Dokkyo University School of Medicine, 800 Kitabayashi, Mibu, Tochigi 321-0293, Japan. [15]Hematology/Oncology, Cedars-Sinai Medical Center, 8700 Beverly Boulevard, Los Angeles, California 90048, USA. [16]Department of Genetics, National Research Institute for Child Health and Development, 2-10-1 Okura, Setagaya-ku, Tokyo, 157-8535, Japan. [17]Gunma Children's Medical Center, 779 Shimohakoda, Hokkitsu-machi, Shibukawa-shi, Gunma 377-8577, Japan. [18]Division of Hematology, Internal Medicine, Showa University Fujigaoka Hospital, 1-30 Fujigaoka, Aoba-ku, Yokohama, Kanagawa 227-8501, Japan.
*These authors contributed equally to this work.

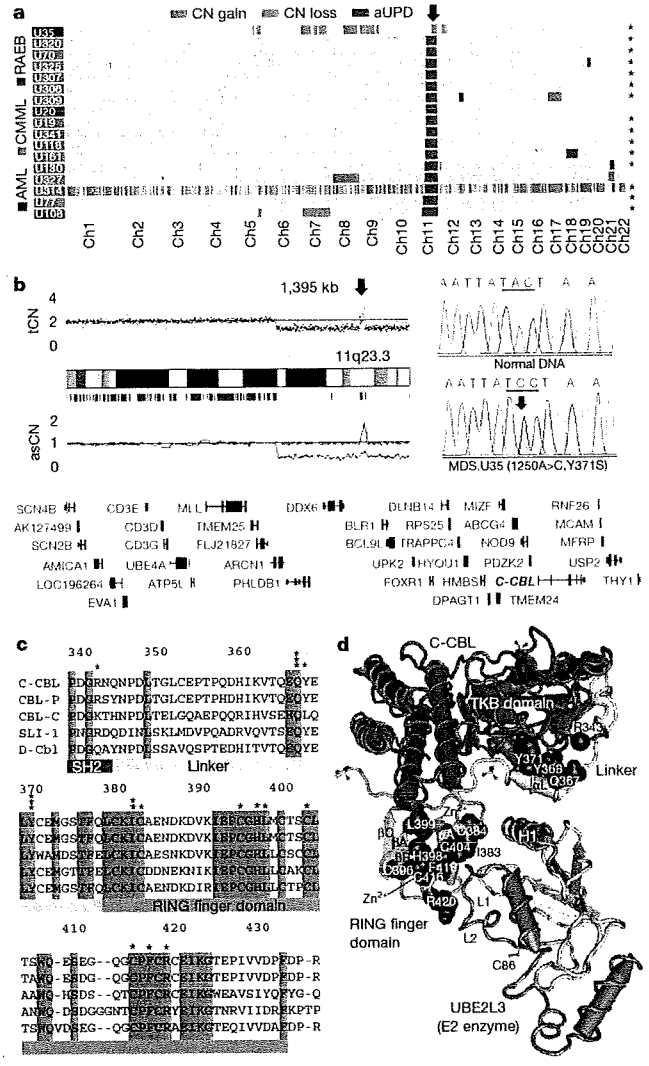

Figure 1 | Common UPD on the 11q arm and *C-CBL* mutations in myeloid neoplasms. **a**, Copy number profiles of 17 cases with myeloid neoplasms showing 11qUPD. Regions of copy number (CN) gains, losses and aUPD are depicted in different colours. Histologies are shown by coloured boxes. Asterisks denote *C-CBL*-mutated cases. Ch, chromosome; RAEB, refractory anaemia with excess blasts. **b**, CNAG output for MDS.U35. Total copy number (tCN) and allele-specific copy number (asCN) plots show a focal copy number gain spanning a 1.4-Mb segment within 3 Mb of an 11q-aUPD region (left), which contained mutated *C-CBL* in MDS.U35 (right). **c**, Alignments of amino acid sequences for human CBL family proteins and their homologues in *Caenorhabditis elegans* (SLI-1) and *Drosophila* (D-Cbl). Amino acid numbering is on the basis of human *C-CBL*. Conserved amino acids are highlighted. Positions of mutated amino acids are indicated by asterisks. Heterozygous mutations are shown in red. **d**, Mutated amino acid positions in the three-dimensional structure of a human C-CBL–UBE2L3 complex. TKB, tyrosine kinase binding domain.

C-CBL is the cellular homologue of the *v-Cbl* transforming gene of the Cas NS-1 murine leukaemia virus[5,12]. It was recently found to be mutated in human AML cases[13–15]. Together with its close homologue, CBL-B, C-CBL is thought to be involved in the negative modulation of tyrosine kinase signalling, primarily through their E3 ubiquitin ligase activity that is responsible for the downregulation of activated tyrosine kinases[3–5]. By sequencing all *C-CBL* exons in all 222 samples, we found *C-CBL* mutations in 15 of the 17 cases with 11q-aUPD, whereas only 3 out of 205 cases without 11q-aUPD had *C-CBL* mutations, showing a strong association of *C-CBL* mutations with 11q-aUPD ($P = 1.46 \times 10^{-18}$) (Supplementary Fig. 6 and Supplementary Tables 6 and 7), as also indicated in a recent report[16]. Thus, *C-CBL* was thought to be the major, if not the only, target of 11q-aUPD in myeloid neoplasms. Two different *C-CBL* mutations co-existed in three cases (Supplementary Fig. 6b). Somatic origins of the mutations were confirmed in three evaluable cases (Supplementary Fig. 6c).

In most cases, *C-CBL* mutations were missense, involving the evolutionarily conserved amino acids within the linker-RING finger domain that is central to the E3 ubiquitin ligase activity[17] (Fig. 1c). Another case with a predominant Cys384Tyr mutation also contained a nonsense mutation (Arg343X) in a minor subclone, which resulted in a v-Cbl-like truncated protein (Supplementary Fig. 6b). In the remaining two cases, mutations led to amino acid deletions (Δ369−371 and Δ368−382) involving the highly conserved α-helix (αL) of the linker domain and the first loop of the RING finger. According to the published crystal structure of *C-CBL*[17], most of the mutated or deleted amino acids were positioned on the interface for the binding to the E2 enzyme (Fig. 1d), making contact with either the tyrosine kinase binding domain (Tyr 368 and Tyr 371) or E2 ubiquitin-conjugating enzymes (Ile 383, Cys 404 and Phe 418). Especially, all seven linker-domain mutations selectively involved just three amino acids (Gln 367, Tyr 368 and Tyr 371) within the conserved αL helix (Fig. 1d). Mutations were clearly homozygous in nine cases, and the apparently heterozygous chromatograms in the other six cases could also be compatible with homozygous mutations affecting the aUPD-positive tumour clones, given the presence of substantial normal cell components within these samples. Mutations in the remaining three cases were considered to be heterozygous. About half of the *C-CBL*-mutated cases carried coexisting mutations of *RUNX1* (four cases), *TP53* (one case), *FLT3* internal tandem duplication (1 case) or *JAK2* (3 cases). *NRAS* and *KRAS* mutations were prevalent among CMML (15.1%) but occurred within discrete clusters from *C-CBL*-mutated cases (Supplementary Tables 2 and 6 and Supplementary Fig. 5). The mutation status of *C-CBL* did not substantially affect the clinical outcome (Supplementary Fig. 7).

All tested *C-CBL* mutants induced clear oncogenic phenotypes in NIH3T3 fibroblasts, as demonstrated by enhanced colony formation in soft agar and tumour generation in nude mice (Supplementary Fig. 8). Transformed NIH3T3 cells showed PI3 kinase-dependent activation of Akt and the transformed phenotype was reverted by treatment with the PI3 kinase inhibitor Ly294002 (Supplementary Fig. 9). When introduced into Lin^- $Sca1^+$ $c\text{-}Kit^+$ (LSK) HSPCs, C-CBL mutants (C-CBL(Gln367Pro) and C-CBL(Tyr371Ser)), as well as a mouse lymphoma-derived oncogenic mutant (C-CBL(70Z)), significantly promoted the replating capacity of these progenitors (Fig. 2a). Because c-Cbl negatively modulates tyrosine kinase signalling, and all *C-CBL* mutations, including those previously reported[13–16], affected the critical domains for its enzymatic activity involved in this modulation, C-CBL was postulated to have a tumour suppressor function; loss-of-function could be a mechanism for the oncogenicity of these C-CBL mutants[3,5]. To assess this possibility and to clarify further the role of *C-CBL* mutations in the pathogenesis of myeloid neoplasms, we generated *c-Cbl*$^{-/-}$ mice and examined their haematological phenotypes (Supplementary Fig. 10).

In agreement with previous reports[18–20], *c-Cbl*$^{-/-}$ mice exhibited splenomegaly and an augmented haematopoietic progenitor pool, as was evident from the increased colony formation of bone marrow cells in methylcellulose culture and higher numbers of LSK and CD34-negative LSK cells in bone marrow and/or spleen compared to their wild-type littermates (Fig. 2b–d and Supplementary Fig. 11). Furthermore, when introduced into a *BCR-ABL* transgenic background[21], the *c-Cbl*$^{-/-}$ allele accelerated blastic crisis depending on the allele dosage (Fig. 2e, f). These observations supported the notion that wild-type *C-CBL* has tumour suppressor functions, whereas 'mutant' *C-CBL* acts as an oncogene; *C-CBL* can therefore be both a proto-oncogene and a tumour suppressor gene.

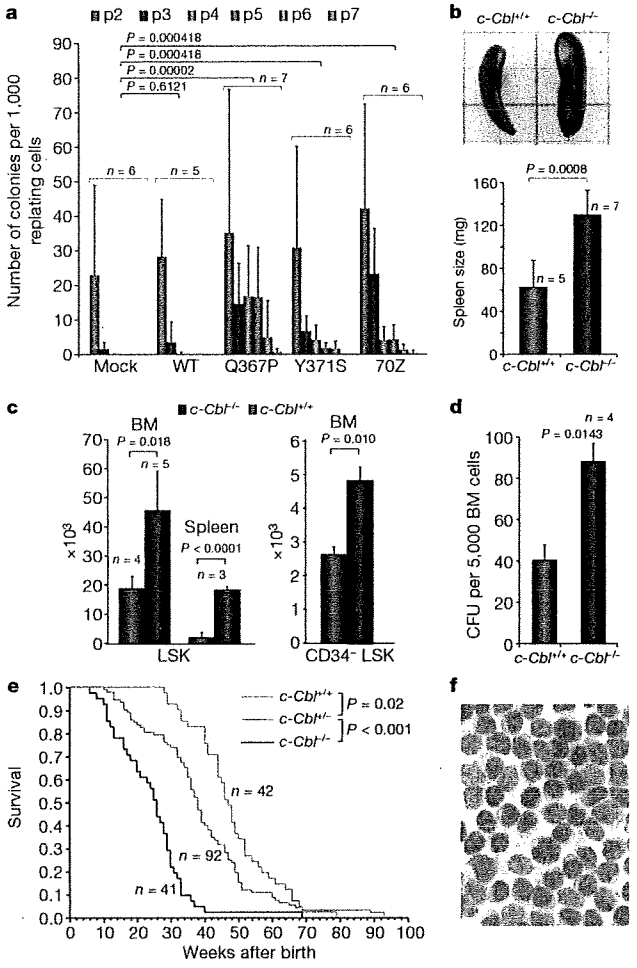

Figure 2 | Tumour-suppressor functions of wild-type C-CBL. **a**, Prolonged replating capacity of LSK cells transduced with mutant *C-CBL* (*C-CBL*(Gln367Pro) and *C-CBL*(Tyr371Ser)), compared to mock- or wild-type *C-CBL*-transduced cells. Replating capacity in methylcellulose culture is shown as mean colony number (and s.d.) per 1,000 replating cells at indicated times of replating. p, passage. **b**, Increased spleen mass in *c-Cbl*$^{-/-}$ mice compared to *c-Cbl*$^{+/+}$ mice (mean spleen weight and s.d.). **c**, Mean number of total LSK (left) and CD34-negative LSK (right) cells (plus s.d.) in bone marrow (BM) and/or spleen in *c-Cbl*$^{+/+}$ (blue columns) and *c-Cbl*$^{-/-}$ mice (red columns). Bone marrow cells from bilateral tibias and femurs were counted for each mouse. **d**, Augmented colony-forming potential of bone marrow cells from *c-Cbl*$^{-/-}$ mice (mean colony number and s.d. per 5,000 bone marrow cells). CFU, colony-forming units. **e**, Kaplan–Meier survival curves of *c-Cbl*$^{+/+}$, *c-Cbl*$^{+/-}$ and *c-Cbl*$^{-/-}$ mice carrying a *BCR-ABL* transgene, showing acceleration of blastic crisis in *c-Cbl*$^{+/-}$ and *c-Cbl*$^{-/-}$ mice. **f**, Wright–Giemsa staining of an enlarged lymph node in a *Bcr-Abl*$^{+}$ *c-Cbl*$^{-/-}$ mouse during blastic crisis shows massive infiltrates of immature leukaemic blasts. Original magnification, ×600.

Mouse LSK HSPCs expressed two Cbl family member proteins: wild-type c-Cbl and Cbl-b (Supplementary Fig. 12)[22]. When transduced into NIH3T3 cells stably expressing human epidermal growth factor receptor (EGFR), both Cbl proteins enhanced ubiquitination of EGFR after EGF stimulation, which was suppressed by coexpression of the C-CBL mutants (Fig. 3a, b). In haematopoietic cells, overexpression of wild-type C-CBL enhanced ligand-induced ubiquitination of a variety of tyrosine kinases, including c-KIT, FLT3 and JAK2. In contrast, C-CBL mutants not only showed compromised enzymatic activity, but also inhibited the ubiquitinating activities in these haematopoietic cells (Fig. 3c), leading to prolonged tyrosine kinase activation after ligand stimulation (Fig. 3d).

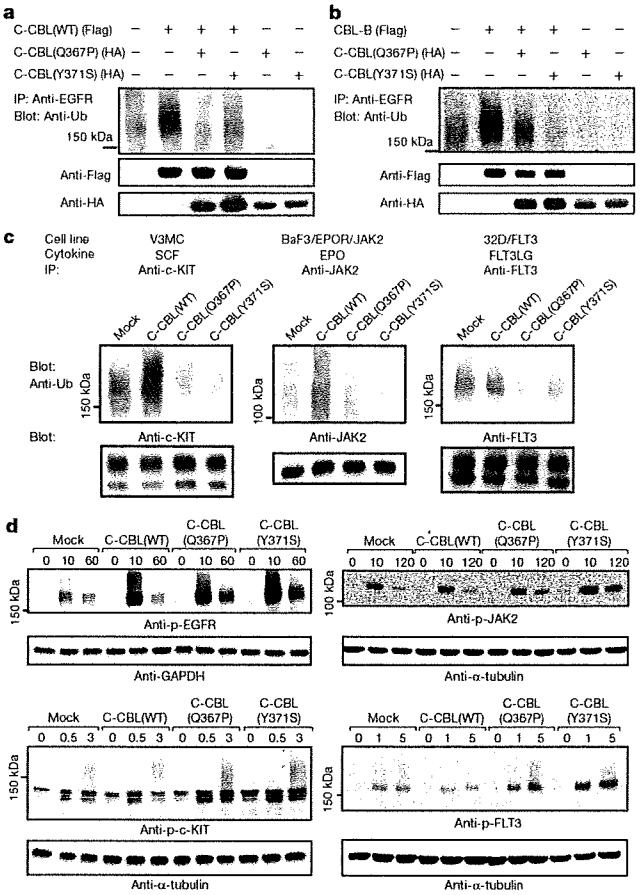

Figure 3 | Inhibitory actions of C-CBL mutants on wild-type C-CBL. **a**, **b**, Flag-tagged wild-type C-CBL (**a**) or CBL-B (**b**) were transfected into NIH3T3 cells stably transduced with human EGFR plus indicated HA-tagged C-CBL mutants. Anti-ubiquitin blots of immunoprecipitated EGFR after EGF stimulation show the inhibitory actions of the C-CBL mutants on ubiquitinating activity of C-CBL (**a**) and CBL-B (**b**). Bottom panels are anti-HA and anti-Flag blots of total cell lysates. **c**, Effects of wild-type and mutant C-CBL on cytokine-induced ubiquitination of c-KIT, JAK2 and FLT3 in haematopoietic cells V3MC, BaF3 co-transduced with human erythropoietin receptor (EPOR) and JAK2 (BaF3/EPOR/JAK2), and FLT3-transduced 32D (32D/FLT3), respectively. Each cell line was further transduced with indicated C-CBL mutants, and ubiquitination of immunoprecipitated kinases was detected by anti-ubiquitin blots at 1 min after stimulation with SCF, EPO and FLT3LG. Anti-kinase blots of the precipitated kinases are shown below each panel. **d**, Kinase phosphorylation was examined at indicated time points (shown in minutes) after ligand stimulation using immunoblot analyses of total cell lysates using antibodies to phosphorylated (p-) EGFR, c-KIT, JAK2 and FLT3 in which anti-α-tubulin or anti-GAPDH blots are provided as a control.

Because tyrosine kinase signalling is central to cytokine responses in haematopoietic cells and its deregulation is a common feature of myeloproliferative disorders[23], we next examined the effects of *C-CBL* mutations (*C-CBL*(Gln367Pro) and *C-CBL*(Tyr371Ser)) and the loss of wild-type *C-CBL* alleles on the responses of LSK HSPCs to various cytokines. In serum-free conditions, *c-Cbl*$^{-/-}$ LSK cells showed a modestly enhanced proliferative response to a variety of cytokines, including SCF, IL3 and TPO, compared to *c-Cbl*$^{+/+}$ cells (mock columns in Fig. 4a). However, the enhanced response in *c-Cbl*$^{-/-}$ cells was markedly augmented and extended to a broader spectrum of cytokines, including FLT3 ligand by the transduction of *C-CBL* mutants. Of note, the effect of *C-CBL* mutant transduction was not remarkable in *c-Cbl*$^{+/+}$ LSK cells except for the response to SCF, which was clearly enhanced by *C-CBL* mutants

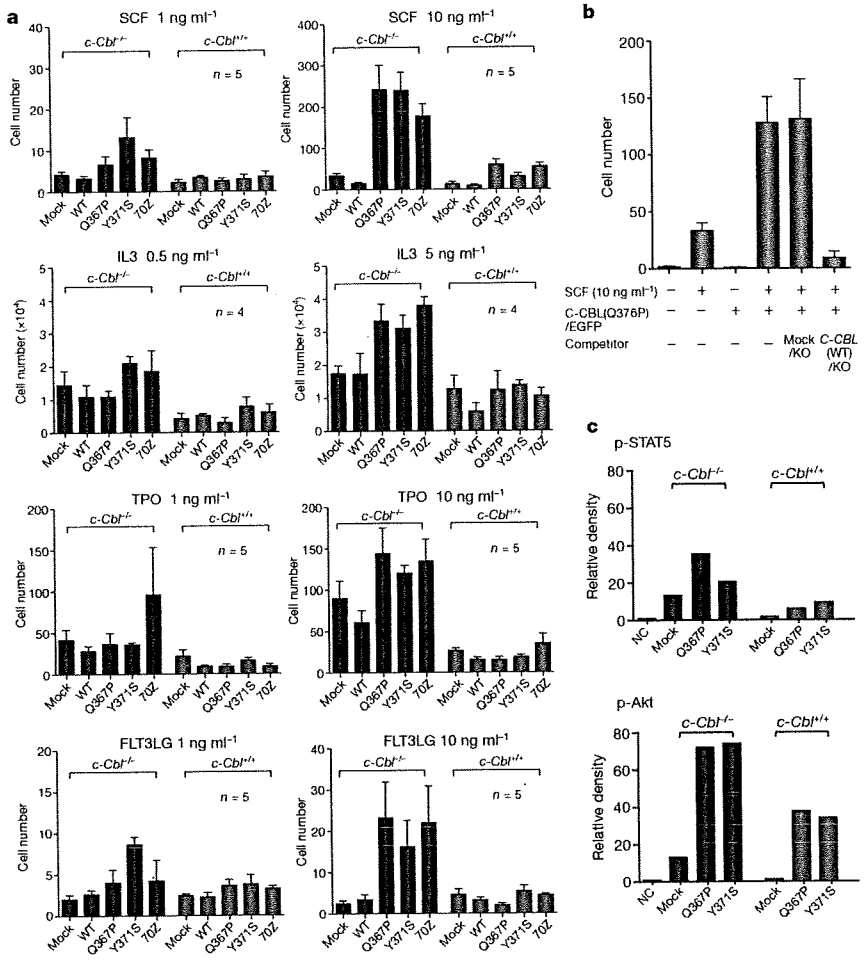

Figure 4 | Gain-of-function of mutant C-CBL augmented by loss of wild-type C-CBL. **a**, *c-Cbl*$^{+/+}$ and *c-Cbl*$^{-/-}$ LSK cells were transfected with various *C-CBL* internal ribosome entry site (IRES)/green fluorescent protein (GFP) constructs, and 50 GFP-positive cells were sorted for serum-free culture containing indicated concentrations of SCF, IL3, TPO and FLT3LG. Mean cell numbers (plus s.e.m.) on day 5 are plotted. **b**, *c-Cbl*$^{-/-}$ LSK cells were co-transduced with C-CBL(Gln367Pro)-IRES-EGFP (C-CBL(Q367P)/EGFP) and mock-IRES-Kusabira-Orange (mock/KO) or wild-type *C-CBL*-IRES-Kusabira-Orange (*C-CBL*(WT)/KO), and 50 GFP/KO double-positive cells were sorted into each well for cell proliferation assays in serum-free culture containing 10 ng ml^{-1} SCF. Mean cell numbers on day 5 (plus s.e.m., $n = 5$) are plotted. **c**, Ten thousand *c-Cbl*$^{+/+}$ and *c-Cbl*$^{-/-}$ LSK cells transduced with various C-CBL constructs were stimulated with 10 ng ml^{-1} SCF and 10 ng ml^{-1} TPO for 15 min. Total cell lysates were analysed by immunoblotting, using antibodies to STAT5, Akt and their phosphorylated forms. The intensities of phosphorylated proteins relative to total STAT5 (top panel) and Akt (bottom panel) are plotted. NC indicates the mean background signal obtained with nonspecific IgG.

even with a *c-Cbl*$^{+/+}$ background (Fig. 4a and Supplementary Fig. 13). To clarify further the effect of wild-type C-CBL on C-CBL mutants, both wild-type C-CBL and C-CBL mutants were co-transduced into *c-Cbl*$^{-/-}$ LSK cells, and their effects on the response to SCF were examined. As shown in Fig. 4b, the hyperproliferative response induced by C-CBL mutants was almost completely abolished by the co-transduction of wild-type C-CBL, suggesting the pathogenic importance of loss of wild-type *C-CBL* alleles found in most *C-CBL*-mutated cases. LSK cells transduced with C-CBL mutants also showed enhanced activation of the STAT5 and Akt pathways on cytokine stimulation (SCF and TPO), which was more pronounced in *c-Cbl*$^{-/-}$ than *c-Cbl*$^{+/+}$ LSK cells (Fig. 4c and Supplementary Fig. 14).

The modest enhancement of sensitivity to cytokines found in *c-Cbl*$^{-/-}$ LSK cells was a consequence of loss of C-CBL functions. In contrast, the hypersensitive response of mutant-transduced *c-Cbl*$^{-/-}$ LSK cells to a broad spectrum of cytokines represents gain-of-function of the mutants that could not be ascribed to a simple loss of C-CBL functions, which was also predicted from the strong association of *C-CBL* mutations with 11q-aUPD by analogy to the gain-of-function *JAK2* mutations associated with 9p-aUPD in polycythemia vera[2]. The gain-of-function of C-CBL mutants became more evident under a *c-Cbl*$^{-/-}$ background. The hypersensitive response to cytokines induced by mutant C-CBL under the *c-Cbl*$^{-/-}$ background was largely offset by the presence of the wild-type *c-Cbl* allele or by the transduction of the wild-type C-CBL gene, suggesting that the gain-of-function could be closely related to loss of C-CBL-like functions, probably by inhibition of Cbl-b. Supporting this view is a previous report that *c-Cbl/Cbl-b* double knockout T cells showed more profound impairments in the downregulation of the T-cell receptor (TCR), more sustained TCR signalling, and more vigorous proliferation, than *c-Cbl* or *Cbl-b* single knockout T cells after anti-CD3 (also known as CD3e) stimulation[24]. This is analogous to the gain-of-function found in some TP53 mutants, which has been explained by functional inhibition of two TP53 homologues, TP73 and TP63 (refs 25, 26). Of note, TP53 was also originally isolated as an oncogene through its mutated forms[27]. The Cbl-b inhibition-based gain-of-function model could be tested directly by comparing the behaviour of *c-Cbl/Cbl-b* double knockout LSK cells with that of LSK cells carrying homozygously knocked-in mutant *C-CBL* alleles. On the other hand, there remains a possibility that the gain-of-function could be mediated by a mechanism other than the simple inhibition of the homologue, because C-CBL mutants retained several motifs

that interacted with numerous signal-transducing molecules. Furthermore, considering the ubiquitous expression of CBL proteins, it would be of interest to explore the possible involvement of mutations in all *CBL* family members in other human cancers.

METHODS SUMMARY

Genomic DNA from 222 bone marrow samples with myeloid neoplasms were analysed using GeneChip SNP-genotyping microarrays (Affymetrix GeneChip) as described[28]. Allelic imbalances were detected from the allele-specific copy numbers calculated using CNAG/AsCNAR software (http://www.genome.umin.jp)[9,10]. *C-CBL* mutations were examined by sequencing PCR-amplified genomic DNA. For functional assays, haemagglutinin (HA)- or Flag-tagged complementary DNAs of wild-type and mutant *C-CBL* were generated by *in vitro* mutagenesis, constructed into a MSCV-based retroviral vector, pGCDNsamIRESGFP or pGCDNsamIRESKO, and used for retrovirus-mediated gene transfer. For the evaluation of oncogenicity of C-CBL mutants, NIH3T3 cells were transfected with various *C-CBL* constructs and used for colony assays in soft agar and tumour formation assays in nude mice. *c-Cbl*-deficient mice were generated using a conventional strategy of gene-targeting and crossed with *BCR-ABL* transgenic mice to evaluate the effect of the *c-Cbl*$^{-}$ allele on the acceleration of blastic crisis. LSK cells sorted from *c-Cbl*$^{+/+}$ and *c-Cbl*$^{-/-}$ mice were transduced with various *C-CBL* constructs. Their responses to cytokines were evaluated by cell proliferation assays, followed by immunoblot analyses of c-KIT, FLT3 and JAK2, as well as their downstream signalling molecules. The effects of C-CBL mutant expression on the ubiquitination of EGFR, c-KIT, FLT3 and JAK2 were examined by transducing C-CBL mutants into relevant cells, followed by anti-ubiquitin blots of the immunoprecipitated kinases after ligand stimulation. Functional competition of C-CBL mutants with wild-type C-CBL was assessed by cell proliferation assays of LSK cells co-transduced with both wild-type and mutant C-CBL genes. This study was approved by the ethics boards of the University of Tokyo, Chang Gung Memorial Hospital and Showa University. Antibodies and primers used in this study are listed in Supplementary Tables 8 and 9.

Full Methods and any associated references are available in the online version of the paper at www.nature.com/nature.

Received 9 October 2008; accepted 30 June 2009.
Published online 20 July 2009.

1. Knudson, A. G. Two genetic hits (more or less) to cancer. *Nature Rev. Cancer* 1, 157–162 (2001).
2. James, C. *et al.* A unique clonal JAK2 mutation leading to constitutive signalling causes polycythaemia vera. *Nature* 434, 1144–1148 (2005).
3. Ryan, P. E. *et al.* Regulating the regulator: negative regulation of Cbl ubiquitin ligases. *Trends Biochem. Sci.* 31, 79–88 (2006).
4. Schmidt, M. H. & Dikic, I. The Cbl interactome and its functions. *Nature Rev. Mol. Cell Biol.* 6, 907–918 (2005).
5. Thien, C. B. & Langdon, W. Y. Cbl: many adaptations to regulate protein tyrosine kinases. *Nature Rev. Mol. Cell Biol.* 2, 294–307 (2001).
6. Thien, C. B. & Langdon, W. Y. c-Cbl and Cbl-b ubiquitin ligases: substrate diversity and the negative regulation of signalling responses. *Biochem. J.* 391, 153–166 (2005).
7. Corey, S. J. *et al.* Myelodysplastic syndromes: the complexity of stem-cell diseases. *Nature Rev. Cancer* 7, 118–129 (2007).
8. Jaffe, E., Harris, N., Stein, H. & Vardiman J. *World Health Organization Classification of Tumours: Pathology and Genetics of Tumours of Haematopoietic and Lymphoid Tissues* 62–73 (IARC Press, 2002).
9. Nannya, Y. *et al.* A robust algorithm for copy number detection using high-density oligonucleotide single nucleotide polymorphism genotyping arrays. *Cancer Res.* 65, 6071–6079 (2005).
10. Yamamoto, G. *et al.* Highly sensitive method for genomewide detection of allelic composition in nonpaired, primary tumor specimens by use of affymetrix single-nucleotide-polymorphism genotyping microarrays. *Am. J. Hum. Genet.* 81, 114–126 (2007).
11. Haase, D. Cytogenetic features in myelodysplastic syndromes. *Ann. Hematol.* 87, 515–526 (2008).
12. Langdon, W. Y. *et al.* v-cbl, an oncogene from a dual-recombinant murine retrovirus that induces early B-lineage lymphomas. *Proc. Natl Acad. Sci. USA* 86, 1168–1172 (1989).
13. Abbas, S. *et al.* Exon 8 splice site mutations in the gene encoding the E3-ligase CBL are associated with core binding factor acute myeloid leukemias. *Haematologica* 93, 1595–1597 (2008).
14. Caligiuri, M. A. *et al.* Novel c-CBL and CBL-b ubiquitin ligase mutations in human acute myeloid leukemia. *Blood* 110, 1022–1024 (2007).
15. Sargin, B. *et al.* Flt3-dependent transformation by inactivating c-Cbl mutations in AML. *Blood* 110, 1004–1012 (2007).
16. Dunbar, A. J. *et al.* 250K single nucleotide polymorphism array karyotyping identifies acquired uniparental disomy and homozygous mutations, including novel missense substitutions of c-Cbl, in myeloid malignancies. *Cancer Res.* 68, 10349–10357 (2008).
17. Zheng, N. *et al.* Structure of a c-Cbl-UbcH7 complex: RING domain function in ubiquitin-protein ligases. *Cell* 102, 533–539 (2000).
18. Murphy, M. A. *et al.* Tissue hyperplasia and enhanced T-cell signalling via ZAP-70 in c-Cbl-deficient mice. *Mol. Cell. Biol.* 18, 4872–4882 (1998).
19. Naramura, M. *et al.* Altered thymic positive selection and intracellular signals in Cbl-deficient mice. *Proc. Natl Acad. Sci. USA* 95, 15547–15552 (1998).
20. Rathinam, C. *et al.* The E3 ubiquitin ligase c-Cbl restricts development and functions of hematopoietic stem cells. *Genes Dev.* 22, 992–997 (2008).
21. Honda, H. *et al.* Acquired loss of p53 induces blastic transformation in p210(bcr/abl)-expressing hematopoietic cells: a transgenic study for blast crisis of human CML. *Blood* 95, 1144–1150 (2000).
22. Zeng, S. *et al.* Regulation of stem cell factor receptor signaling by Cbl family proteins (Cbl-b/c-Cbl). *Blood* 105, 226–232 (2005).
23. Kaushansky, K. Hematopoietic growth factors, signaling and the chronic myeloproliferative disorders. *Cytokine Growth Factor Rev.* 17, 423–430 (2006).
24. Naramura, M. *et al.* c-Cbl and Cbl-b regulate T cell responsiveness by promoting ligand-induced TCR down-modulation. *Nature Immunol.* 3, 1192–1199 (2002).
25. Dittmer, D. *et al.* Gain of function mutations in p53. *Nature Genet.* 4, 42–46 (1993).
26. Lang, G. A. *et al.* Gain of function of a p53 hot spot mutation in a mouse model of Li-Fraumeni syndrome. *Cell* 119, 861–872 (2004).
27. Finlay, C. A., Hinds, P. W. & Levine, A. J. The p53 proto-oncogene can act as a suppressor of transformation. *Cell* 57, 1083–1093 (1989).
28. Chen, Y. *et al.* Oncogenic mutations of ALK kinase in neuroblastoma. *Nature* 455, 971–974 (2008).

Supplementary Information is linked to the online version of the paper at www.nature.com/nature.

Acknowledgements This work was supported by the Core Research for Evolutional Science and Technology, Japan Science and Technology Agency, a Grant-in-Aid from the Ministry of Health, Labor and Welfare of Japan and from the Ministry of Education, Culture, Sports, Science and Technology, and a grant from National Health Research Institute, Taiwan, NHRI-EX96-9434SI, and NIH-2R01CA026038-30. We thank W. Y. Langdon for providing a human *C-CBL* cDNA. A mast-cell cell line expressing c-KIT V3MC was a gift from M. F. Gurish. We also thank Y. Ogino and K. Fujita for their technical assistance.

Author Contributions M.S. and M.Kato performed microarray experiments and subsequent data analyses. T.S., T.Y., H.Honda and H.Hirai generated and analysed *c-Cbl*-null mice. M.S., M.Otsu, S.Y., M.N., K.K., N.G., M.Onodera, M.S.-Y. and H.N. conducted functional assays of C-CBL mutants. L.-Y.S., M.S., M.Kato, K.N., J.T. and A.T. performed mutation analysis. H.O. performed pathological analysis of *c-Cbl*-null mice. L.-Y.S., N.K., H.Harada, M.Kurokawa, S.C., H.M., H.P.K. and M.Omine prepared MDS specimens. M.S., M.Otsu, Y.H., K.O., H.M., H.N., L.-Y.S., H.P.K. and S.O. designed the overall study, and S.O. wrote the manuscript. All authors discussed the results and commented on the manuscript.

Author Information Full copy number data for the 222 samples are accessible from the Gene Expression Omnibus public database (http://ncbi.nlm.nih.gov/geo/) with the accession number GSE15187. Reprints and permissions information is available at www.nature.com/reprints. Correspondence and requests for materials should be addressed to S.O. (sogawa-tky@umin.ac.jp) or L.-Y.S. (sly7012@adm.cgmh.org.tw).

METHODS

Genome-wide analysis of allelic imbalances in primary myeloid neoplasms. Bone marrow specimens were obtained from 222 patients diagnosed with myeloid neoplasms according to the WHO classification (Supplementary Tables 1 and 2). High molecular weight genomic DNA was extracted and used for microarray analysis using Affymetrix GeneChip 50K XbaI, HindIII or 250K NspI, according to the manufacturer's instructions. Genome-wide detection of allelic imbalances was performed using CNAG/AsCNAR software (http://www.genome.umin.jp)[9,10].

Mutation analysis. Mutation analysis was performed by direct sequencing of PCR-amplified coding exons of the relevant genes, using an ABI PRISM 3100 genetic analyser (Applied Biosystems). The target genes, exons and PCR primers are listed in Supplementary Table 8. Tandem duplication of the *FLT3* gene was examined by genomic PCR and sequencing.

Preparation of high-titre vesicular stomatitis virus glycoprotein (VSV-G)-pseudotyped retroviral particles. HA-tagged human *C-CBL* cDNA was a gift from W. Y. Langdon. Nine mutant cDNAs of *C-CBL*, including eight from patients' specimens and a 70Z mutant corresponding to a mutant isolated from mouse lymphoma[29], were generated on the basis of this construct, using a QuickChange site-directed mutagenesis kit (Stratagene). These were then constructed into the retrovirus vectors pGCDNsamIRESGFP and pGCDNsamIRESKO[30–32]. Vector plasmids were co-transfected with a VSV-G cDNA into 293GP cells (provided by R. C. Mulligan) to obtain retrovirus-containing supernatant, which was then transduced into 293GPG cells to establish stable cell lines capable of producing VSV-G-pseudotyped retroviral particles on induction[33,34]. The average titre of retrovirus stocks prepared from these cell lines routinely exceeded approximately $1–10 \times 10^7$ inclusion-forming units per ml, as estimated using Jurkat cells.

Assays for anchorage-independent growth and tumorigenicity in nude mice. NIH3T3 cells (the Japan Cell Resource Bank) were stably transduced with wild-type and mutant *C-CBL* by retrovirus-mediated gene transfer. For colony formation assays, 1.0×10^3 stable cells for each construct were inoculated in 0.33% top agar, and the numbers of colonies >1 mm in diameter were counted 3 weeks after inoculation ($n = 8$). Experiments were repeated four times. For tumour formation in nude mice, 1.0×10^7 stable cells were inoculated subcutaneously at two sites per mouse. Cells were inoculated at six sites in three mice for each construct.

Purification of LSK HSPCs. LSK HSPCs were purified from bone marrow and spleen as described[35,36]. Multicolour flow cytometry analysis and cell sorting were performed using a MoFlo cell Sorter (Beckman Coulter). The purity of sorted cell fractions consistently exceeded 98%.

Replating assays of bone marrow progenitor cells. Bone marrow LSK cells were infected with IRES/GFP-containing retrovirus carrying mock, wild-type C-CBL and three C-CBL mutants (C-CBL(Gln367Pro), C-CBL(Tyr371Ser) and C-CBL(Cys384Gly)) as well as C-CBL(70Z) on RetroNectin-coated dishes. After 48 h infection in culture in StemSpan supplemented with SCF (50 ng ml^{-1}; Peprotech), TPO (20 ng ml^{-1}) and FLT3LG (20 ng ml^{-1}), 1.0×10^2 GFP-positive cells were inoculated in MethoCult M3231 supplemented with TPO (20 ng ml^{-1}), IL3 (10 ng ml^{-1}), IL6 (10 ng ml^{-1}), FLT3LG (10 ng ml^{-1}) and SCF (50 ng ml^{-1}) for colony formation. Colony-forming cells were collected 7 days after each inoculation, from which 1.0×10^3 cells were repeatedly subjected to replating until no colonies were produced. Experiments were repeated at the indicated times for each C-CBL construct.

Generation of *c-Cbl*$^{-/-}$ mice and evaluation of their tumour-prone phenotype. *c-Cbl*$^{-/-}$ mice were generated using a conventional method of gene targeting (Supplementary Fig. 10). *c-Cbl*$^{+/+}$, *c-Cbl*$^{+/-}$ and *c-Cbl*$^{-/-}$ mice were crossed with *BCR-ABL* transgenic mice, and their survival and the development of blastic crises were monitored.

Evaluation of haematopoietic pool size in *c-Cbl*$^{-/-}$ mice. LSK and CD34$^-$ LSK cells were sorted from bone marrow cells or spleens of *c-Cbl*$^{-/-}$ mice, and their numbers were compared to those in *c-Cbl*$^{+/+}$ littermates (8 week old). Approximately 5×10^3 bone marrow cells collected from *c-Cbl*$^{+/+}$ and *c-Cbl*$^{-/-}$ mice were inoculated into MethoCult M3231 culture supplemented with TPO (20 ng ml^{-1}), IL3 (10 ng ml^{-1}), IL6 (10 ng ml^{-1}), EPO (3 U ml^{-1}) and SCF (50 ng ml^{-1}). The number of colonies was counted 7 days after culturing.

***In vitro* cell proliferation assays.** Approximately 6×10^3 LSK cells from *c-Cbl*$^{-/-}$ mice and their *c-Cbl*$^{+/+}$ littermates (8 week old) were sorted into RetroNectin-coated 96-well U-bottom plates containing α-minimum essential medium supplemented with 1% fetal bovine serum (FBS), mouse SCF (50 ng ml^{-1}), and human TPO (100 ng ml^{-1}). After 24 h pre-incubation, retrovirus supernatant was added to each well at a multiplicity of infection of about 10. The plates were incubated for another 24 h in the presence of protamine sulphate (10 μg ml^{-1}), followed by repeated infection and extended culture for 2 days in S-Clone SF-O3 medium (Sanko Junyaku) supplemented with 1% BSA, 50 ng ml^{-1} SCF and 50 ng ml^{-1} TPO. On day 4, fluorescent-marker-positive cells were sorted for subsequent analyses. Cell survival and proliferation of LSK cells transduced with different *C-CBL* constructs were assessed in serum-free liquid culture in 96-well U-bottom plates in the presence of various cytokines. Each well received 50 fluorescent-marker-positive LSK cells, and the cells were cultured in S-Clone supplemented with 1% BSA plus SCF, TPO, IL3 or FLT3LG at the indicated concentrations. Cell numbers were counted either by analysing well images or by flow cytometry using FlowCount beads (Beckman Coulter). After 6 h serum starvation, 1×10^4 LSK cells transduced with various *C-CBL* constructs were stimulated with SCF (10 ng ml^{-1}) and TPO (10 ng ml^{-1}) for 15 min. Whole-cell lysates were examined for activation of STAT5 and Akt by immunoblots using the respective antibodies.

Immunoblot analysis of physical interactions between mutant C-CBL and CBL-B. Flag-tagged CBL-B or C-CBL was co-transfected into NIH3T3 cells with each of three HA-tagged C-CBL mutants (C-CBL(Gln367Pro), C-CBL(Tyr371Ser) and C-CBL(70Z)). Total cell lysates of these NIH3T3 cells were immunoprecipitated with anti-Flag antibody, followed by immunoblot analysis with anti-HA antibody.

Detection of ubiquitination and phosphorylation of kinases. After overnight serum starvation, NIH3T3 cells stably transduced with human EGFR, and indicated HA-tagged C-CBL mutants and Flag-tagged wild-type C-CBL were stimulated with human EGF (10 ng ml^{-1}) for 2 min. Cell lysates were immunoprecipitated with anti-EGF antibody, followed by immunoblotting using anti-ubiquitin antibody. Constructs for wild-type C-CBL and mutant C-CBL were stably transduced into a mast cell line, V3MC, FLT3-transduced 32D cells (32D/FLT3) and BaF3 cells transduced with human EPOR and JAK2 (BaF3/EPOR/JAK2) using retrovirus-mediated gene transfer. After overnight serum starvation, the transduced cells were stimulated with 10 ng ml^{-1} SCF (V3MC), 10 U ml^{-1} EPO (BaF3/EPOR/JAK2) or 10 ng ml^{-1} FLT3LG (32D/FLT3) for 1 min. The specific kinases were immunoprecipitated with relevant antibodies, and their ubiquitination was detected by immunoblotting with anti-ubiquitin antibody. Tyrosine phosphorylation of EGFR, c-KIT, JAK2 and FLT3 was examined by immunoblot analyses of total cell lysates after cytokine stimulation at indicated time points, using antibodies specifically recognizing phosphorylated kinases, anti-p-EGFR, anti-p-c-KIT, anti-p-JAK2 and anti-p-FLT3, respectively. Anti-GAPDH or anti-α-tubulin immunoblot was performed as a control. Antibodies used in this study are listed in Supplementary Table 9.

Statistical analysis. Statistical significance of prolonged replating capacity of mutant *C-CBL*-transduced LSK cells was tested by counting the total number of dishes that produced colonies, followed by Fisher's exact test. Survival curves of *c-Cbl*$^{+/+}$, *c-Cbl*$^{+/-}$ and *c-Cbl*$^{-/-}$ mice containing the *BCR-ABL* transgene were generated using the Kaplan–Meier method. Overall survivals of *C-CBL*-mutated and non-mutated CMML cases were analysed according to the proportional hazard model, using STATA software. Statistical differences in survival were evaluated using the log-rank test, and statistical differences in 2×2 contingency tables were tested according to Fisher's exact method. Student's *t*-tests were used to evaluate the significance of difference in spleen mass, number of haematopoietic progenitors and colony-forming cells between *c-Cbl*$^{+/+}$ and *c-Cbl*$^{-/-}$.

29. Blake, T. J. *et al.* The sequences of the human and mouse c-cbl proto-oncogenes show v-cbl was generated by a large truncation encompassing a proline-rich domain and a leucine zipper-like motif. *Oncogene* 6, 653–657 (1991).
30. Hamanaka, S. *et al.* Stable transgene expression in mice generated from retrovirally transduced embryonic stem cells. *Mol. Ther.* 15, 560–565 (2007).
31. Nabekura, T. *et al.* Potent vaccine therapy with dendritic cells genetically modified by the gene-silencing-resistant retroviral vector GCDNsap. *Mol. Ther.* 13, 301–309 (2006).
32. Sanuki, S. *et al.* A new red fluorescent protein that allows efficient marking of murine hematopoietic stem cells. *J. Gene Med.* 10, 965–971 (2008).
33. Ory, D. S., Neugeboren, B. A. & Mulligan, R. C. A stable human-derived packaging cell line for production of high titer retrovirus/vesicular stomatitis virus G pseudotypes. *Proc. Natl Acad. Sci. USA* 93, 11400–11406 (1996).
34. Suzuki, A. *et al.* Feasibility of *ex vivo* gene therapy for neurological disorders using the new retroviral vector GCDNsap packaged in the vesicular stomatitis virus G protein. *J. Neurochem.* 82, 953–960 (2002).
35. Ema, H. *et al.* Adult mouse hematopoietic stem cells: purification and single-cell assays *Nature Protoc.* 1, 2979–2987 (2006).
36. Osawa, M. *et al.* Long-term lymphohematopoietic reconstitution by a single CD34-low/negative hematopoietic stem cell. *Science* 273, 242–245 (1996).

European Journal of Haematology ISSN 0902-4441

ORIGINAL ARTICLE

Aberrant p53 protein expression and function in a panel of hematopoietic cell lines with different p53 mutations

Shimeru Kamihira[1], Chiharu Terada[1], Daisuke Sasaki[1], Katsunori Yanagihara[1], Kunihiro Tsukasaki[2], Hiroo Hasegawa[1], Yasuaki Yamada[1]

Departments of [1]Laboratory Medicine and [2]Hematology, Nagasaki University Graduate School of Biomedical Sciences, Nagasaki, Japan

Abstract

The *p53* gene is one of the most important genes involved in carcinogenesis and its role in part has been clarified by research using cell lines. To know the comprehensive characteristics of 22 hematopoietic cell lines (T, 13 and non-T, nine lines), the relationship between p53 mutational status, its altered functioning, and its mRNA and protein levels were examined. p53 mutations were less frequent in T-cell lines (38% vs. 78%) with mainly single nucleotide substitutions generating missense codons. Of 22 different p53 mutations, 12 (54.5%) resulted in mutated proteins, with the mutations clustering mainly in the sequence-specific DNA-binding site region located from amino acid residues 102 to 292. *p53* mRNA and protein assays determined that wild-type cell lines expressed constant levels of both mRNA and protein, but mutated cell lines demonstrated two expression patterns: protein over-expression with reduced mRNA levels, because of missense mutations; and protein under-expression with little mRNA expression, because of other mutations. The resistance to Nutlin (MDM2 inhibitor)-induced apoptosis was associated with p53 mutations independently of MDM2 expression levels. This clarification of the unique associations in cell lines useful for bio-medical studies will contribute to a better understanding of p53-associated carcinogenesis.

Key words p53; mutation; haplo-insufficiency; hematologic cell line; adult T-cell leukemia

Correspondence Shimeru Kamihira, PhD, MD, Department of Laboratory Medicine, Nagasaki University Graduate School of Biomedical Sciences, 1-7-1, Sakamoto, Nagasaki 852-8501, Japan. Tel: +81 95 819 7407; Fax: +81 95 819 7422; e-mail: kamihira@nagasaki-u.ac.jp

Accepted for publication 22 December 2008

doi:10.1111/j.1600-0609.2009.01211.x

The tumor suppressor gene *p53* is located on the short arm of chromosome 17 and plays a central role in control of the cell cycle, DNA repair, and activation of apoptosis. Abrogation of these *p53* functions is thought to be involved in carcinogenesis (1, 2). *p53* knockout mice have an increased tendency to develop spontaneous tumors. It was previously thought that transformation required the inactivation of both *p53* alleles, i.e., loss of heterozygosity, but recent studies have shown that *p53* function can also be disrupted by haplo-insufficiency; i.e., the alteration of one allele of the gene with the other allele remaining normal (3). Inactivation of the *p53* gene is known to be caused by genetic and epigenetic mechanisms, such as mutation, methylation, and interaction with viral proteins. *p53* alterations are widely observed in at least 50% of human tumors, including hematologic malignancies, with colon, breast, and lung cancers having the highest frequencies of *p53* mutations (2, 4).

Mutant p53 proteins encoded by mutated alleles have several characteristics that differ from those of wild-type p53, including a longer half-life and a dominant negative effect on wild-type p53. Furthermore, the dominant negative function seems to vary according to the polymorphic status of codon 72 (C466G; arginine vs. proline) (5). These characteristics of the mutant protein appear to account for its over-expression in tumor cells harboring the mutated gene, and which demonstrate biologically aggressive behavior and chemoresistance (6–8). The presence of *p53* mutations and over-expression of p53 protein has a strong prognostic impact (9, 10). Several studies

have reported that adult T-cell leukemia (ATL) patients demonstrate mutational inactivation of p53 in 20–40% of cases, and that gene inactivation contributes to the development of malignant phenotypes (11).

The Nutlins, *cis*-imidazoline analogs, are novel small-molecule inhibitors of MDM2, which bind to MDM2, releasing them from negative control by the p53 pathway and leading to effective p53 stabilization and activation in wild-type cells (12). However, little is known about the association between *p53* mutational status and expression levels and functioning of p53 protein. Accordingly, using a panel of hematopoietic cell lines available as bio-source to study oncology, we examined the associations between *p53* mutations, p53 functional status, and mRNA and protein levels.

Materials and methods

Cell lines

The hematopoietic cell lines used included six ATL-derived T-cell lines, three human T-cell leukemia virus type-1 (HTLV-1)-infected T-cell lines, four T-cell lines without HTLV-1, five lymphoma-derived B-cell lines, two monocytic cell lines, and two others. All but three (MT1, MT2, and HUT102) of the ATL cell lines were established in our laboratory (13). The other cell lines were obtained from the American Type Culture Collection (Rockville, MD, USA), and the Hayashibara Bio Inc (Okayama, Japan). Each cell line was cultured according to the supplier's, or our, protocols.

High molecular weight DNA was extracted from cell lines using a QIAmp DNA Blood Mini kit (Qiagen GmbH, Hilden, Germany). Total RNA was extracted using ISOGEN (Nippon Gene, Toyama, Japan). After removing contaminating genomic DNA using a Message Clean kit, cDNA was synthesized using Oligo (dT) 12–18 Primer and SuperScript III Reverse Transcriptase (Invitrogen Corp., Carlsbad, CA, USA). All primers and probes used in this study were designed using Primer3Plus (14) (The sequences of all primers and probes used here are available via an e-mail of kamihira@nagasaki-u.ac.jp).

Mutational analysis

A 1376-bp fragment including the *p53* mRNA open reading frame (ORF) was amplified by polymerase chain reaction (PCR) using primers S1 and AS1. The standard thermal cycling conditions were an initial 98°C for 30 s followed by 35 cycles at 98°C for 10 s and 67°C for 1 min. The amplicons were subjected to direct sequencing analysis to identify mutations in the *p53* ORF. The PCR primers used for cycle sequencing were S1, S2, and S3 for anti-sense products, and AS1, AS2, and AS3 for sense products. Cycle sequencing was performed using a BigDye Terminator v3.1 Cycle Sequencing Kit (Applied Biosystems, Foster City, CA, USA) and an Automated DNA Sequence Analyzer (Model 3100; Applied Biosystems, Foster City, CA, USA). Sequence data for the *p53* ORF region were compared with the published *p53* mRNA sequence (NM_00546).

Real time RT-PCR quantification for *p53* and *mdm2* mRNA levels

Primers and TaqMan probes labeled with TAMRA dye at the 3′ end and FAM at the 5′ end were designed. The mRNA levels for *p53*, *mdm2*, and porphobilinogen deaminase (*PBGD*) were measured from a cDNA template using a LightCycler480 PCR System (Roche Diagnostics, Mannheim, Germany). Briefly, reactions were performed in a 20 μL volume with 5 μL 1/10 diluted cDNA, 0.5 μM PCR primers, 0.1 μM TaqMan probes, and 10 μL of 20 LightCycler 480 probes (Master Mix; Roche Diagnostics). The PCR program consisted of 95°C for 5 min followed by 50 cycles of 95°C for 10 s and 60°C for 30 s. After 50 cycles, the absolute amounts of *p53*, *mdm2*, and *PBGD* mRNA were interpolated from the standard curves generated by the dilution method using plasmids derived from a clone transfected with pTAC-1 Vector (BioDynamics Laboratory Inc., Tokyo, Japan) containing amplicons from the *p53*, *mdm2*, and *PBGD* genes, respectively. To normalize these results for variability in concentration and integrity of RNA and cDNA, the *PBGD* gene was used as an internal control in each sample.

Measurement of p53 protein

Total p53 protein in cell lysates (10 μg) was measured using the Luminex$^{100™}$ System (Hitachi Software Engineering Co., Tokyo, Japan), and the total p53 Antibody Bead Kit (LHO0151, Biosource International, Camarillo, CA, USA), according to the manufacturers' instructions. In brief, cells were washed three times with phosphate-buffered saline and pelleted cells were homogenized at 4°C in lysis buffer (0.1% sodium dodecyl sulfate, 1% Igepal CA-630, and 0.5% sodium deoxycholate) and a protease inhibitor cocktail (Sigma, St Louis, MO, USA). Sample solutions appropriately diluted with assay diluent were incubated with anti-p53 antibody-coupled beads for 2 h at room temperature on an orbital plate shaker, washed three times with wash solution, and the beads were further incubated with biotinylated detector antibody for 1 h. This was followed by incubation with streptavidin-R-phycoerythrin for 30 min at room temperature, and washing, after which the suspended beads were analyzed using the Luminex$^{100™}$ System. A

standard curve was created using serially diluted recombinant p53, and the p53 concentrations in samples were estimated.

Assays for p53 activation

The degree of DNA-binding capacity and the phosphorylation at serine 15 ($p53^{ser15}$) were analyzed as markers of p53 activation, using a TransAM™ p53 Transcription Factor Assay kit (Active Motif, Carlsbad, CA, USA) and an anti-phospho-$p53^{ser15}$/total p53 Multiplex Bead-based system (BioSource International) available for Luminex technology. The degree of activation was demonstrated by the fold induction of the DNA-binding capacity of p53 and the fold induction of phosphorylation of $p53^{ser15}$, relative to the measures before and after treatment with Nutlin-3.

Briefly, nuclear extracts from cells treated with 10 μM Nutlin-3 (Sigma Aldrich, St Louis, MO, USA) for 24 h were diluted in 10 μg of total protein with lysis buffer and applied to plates with immobilized oligonucleotides containing the p53 consensus binding site. After 1 h at room temperature, plates were washed and incubated with p53 antibody, followed by secondary antibody and developing solution. Color generated as a marker of the DNA-binding capacity was read at 450 nm. The procedure was performed according to instructions for the TransAM™ p53 and the Luminex$^{100™}$.

The phosphorylation of $p53^{ser15}$ was analyzed using anti-p53 and anti-phospho $p53^{ser15}$ according to the Luminex$^{100™}$ system protocol, as described above. The final outcome of p53 activation was determined by the degree of apoptosis induced by Nutlin-3 using the annexin V/propidium iodide double staining flow-cytometric method (15).

Statistical analysis

The chi-squared and Fisher's exact tests were used to examine categorical data, and the Mann–Whitney *U*-test

Table 1 Characteristics of cell lines tested and summary of *p53* mutations and deduced amino acid sequences

Cell line	Origin	RT-PCR products	Event				p53 status
			Exon	Codon	Sequence	aa	
SO4	ATL cell	1.4 kb (Arg)[2]	6	223	C919A	Missense (Pro → His)	Mt
ST1	ATL cell	1.4 kb (Pro)					Wt
KK1	ATL cell	1.4 kb (Pro)	3	31	G342A	Missense (Val → Ire)	Mt
			5	152	C706T)	Missense (Pro → Arg)	
KOB	ATL cell	1.4 kb (Pro)					Wt
LM-Y1	ATL cell	1.4 kb (Arg)	4	36	G359A	Silent	Wt
MT1	ATL cell	1.4 kb (Arg)	5	176	G778A	Missense (Cyt → Tyr)	Mt
OMT	HTLV-1 infected T	1.4 kb (Pro)					Wt
MT2	HTLV-1 infected T	1.4 kb (Arg)					Wt
HUT102	HTLV-1 infected T	1.4 kb (Arg)					Wt
MT1s	Non-HTLV-1 T	1.4 kb (Arg)	5	149	C697T	Missense (Ser → Phe)	Mt
MT1g	Non-HTLV-1 T	1.4 kb (Arg)					Wt
MOLT4	Non-HTLV-1 T	1.4 kb (Arg)					Wt
Jurkat	Non-HTLV-1 T	1.4 kb (Arg)	5	125	G626A	Missense (Thr → Arg)	Mt
			6	196	C837T	Nonsense (Stop)	
		1.2 kb (del)	4	59–125	425–625	Deletion 199[1]	
			10	360	1329(G)	Deletion 1[1]	
SuDHL	B-cell lymphoma	1.4 kb (Arg)					Wt
Ramos	B-cell lymphoma	1.4 kb (Arg)	7	254	A/T1011/2G/A	Missense (Ile → Asp)	Mt
SKW6.4	B-cell lymphoma	1.4 kb (Arg)					
		1.2 kb (Pro)	4	59–125	426-624	Deletion 199[1]	Mt
HS-sultan	Myeloma	1.4 kb (Pro)					Wt
CA46	Burkitt lymphoma	1.4 kb (Pro)	7	248	G994A	Missense	Mt
THP1	Monocytic leukemia	1.4 kb (Arg)	5	174–182	770–795	Deletion 25[1]	Mt
U937	Monocytic leukemia	1.4 kb (Arg)	4	105	G564A	Missense (Gly → Ser)	Mt
			5	125	G626A	Silent	
			6	196	C837T	Nonsense (stop)	
		1.2 kb (del)	4	59–125	425–625	Deletion 199[1]	
HL60	Myeloid leukemia	No-detected				Deletion	Mt
K562	Erythroblastic leukemia	1.4 kb (Pro)	5	135	655(C)	Insertion[1]	Mt

[1]Frame shift (stop codon).
[2]p53 codon 72 polymorphic status, C466G.

and Kruskal–Wallis tests were used for non-parametric data. Differences in the strength of the association between two variables were evaluated by the Spearman's rank correlation coefficients. Differences were considered statistically significant when *P*-values were < 0.05.

Results

Mutation profiles of cell lines

Using the present RT-PCR protocol, two main, distinct products of about 1.4 and 1.2 kb were generated in Jurkat, U937, THP1, K562, and SKW6.4 cells, while the remaining 16 cell lines, excluding HL-60 cells, showed a single band of 1.4 kb. No amplified products were observed in HL-60 cells. The results from direct sequencing of the amplicons are summarized in Table 1. Overall, 20 *p53* mutations were identified in 13 of 22 cell lines (59.0%). The mutations were located in exons 3 (one event), 4 (five events), 5 (seven events), 6 (two events), 7 (two events), and elsewhere (two events). Clustering was observed in exons 4 and 6, which is a highly conserved region including the sequence specific DNA-binding sites from amino acids 102 to 292. Of the 20 mutations, 13 (65%) were single nucleotide substitutions, whereas six (30%) were found to be deletions or insertions with frame-shifts generating stop codons. The 13 single nucleotide substitutions consisted of nine missense (69.2%), two nonsense, and two silent mutations. Missense mutations were mainly detected in T-cell lines, whereas deletions and nonsense mutations were mainly detected in B-cell and myeloid cell lines. Fifteen of the 22 mutations, such as C919C, C706T, G342A, G359A, G778A, G778A, C697T, G626A, C626A, C837T, AT1011GA, G994A, 174-182del, G564A, and 655(ins C), were accordant with the previous reports (IARC TP Mutation Database and The TP53 Web site). On the other hand, four kinds of the mutations detected in Jurkat, SKW6.4 and U937 have not yet reported. In particular, 199 base pair deletion (nt 425–625) in exon 4 was detected in only the 1.2 kb PCR products, suggesting that it is derived from a splicing form. Consequently, five of 13 T-cell lines and seven of nine non-T-cell lines (totally 12/22, 54.5%) were deduced to carry mutant p53 proteins. Regarding the relationship between mutations and the genotype of the p53 codon 72 polymorphism (arginine vs. proline), mutations were demonstrated to be in arginine-encoding alleles in nine cell lines, and in proline-encoding alleles in three cell lines, indicating that mutations occurred more frequently in the arginine-encoding alleles (69.2% vs. 23.10%, $P = 0.04$), as shown in Tables 1 and 2.

Association of *p53* mutational status with its mRNA and protein levels

The *p53* mRNA levels differed significantly between the wild-type and the mutated cell lines (0.62 vs. 0.37 $P = 0.048$). The p53 protein levels varied widely from 0 to 15 000 pg/mL, but the mean values were not significantly different between the wild-type and the mutated cell lines (4160 vs. 3860 pg/mL). The p53 protein levels in all cell lines failed to correlate with the p53 mRNA levels, although specific cell lines with protein levels of < 1000 pg/mL showed tendencies toward inverse correlations between *p53* mRNA and protein levels ($r = -0.4636$, the Spearman *U*-test), as shown in Fig. 1. Furthermore, Fig. 1 shows the distinctive distribution of the cell lines which formed three clusters, designated as A, B, and C. Wild-type cell lines clustered in the center area (A), representing balanced expressions of p53

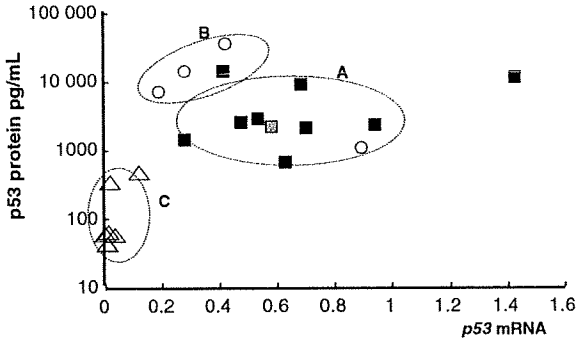

Figure 1 Twin dot graph of p53 protein (*Y*-axis) and mRNA (*X*-axis) expression levels in cell lines categorized according to their *p53* mutational status. Solid square; wild-type, open circle; missense, open triangle; other mutations, gray square; silent mutation. No correlation between *p53* mRNA and protein levels ($r = 0.238$, $P = 0.175$). However, a unique association among the types of mutations, *p53* mRNA and protein was observed, because solid squares are clustered into the central area (A), while mutated cells are separated into two clusters of B and C: The cell lines with wild-type sequences had balanced levels of transcripts and proteins, and cell lines with mutants were subdivided into two groups, with either over-expressed or under-expressed protein levels, with low mRNA expression.

Table 2 Comparison of *p53* codon 72 (C466G) polymorphic status in wild-type and mutated groups

		p53 codon 72 (C466G) status		
p53 mutation	*n* (%)	Arg (%)	Pro (%)	*Unknown (%)*[1]
Wild-type	9 (41.0)	5 (55.5)	4 (45.5)	*0*
Mutated	13 (59.0)	9 (69.2)*	3 (23.1)**	*1 (7.7)*
Total	22 (100)	14	7	*1*

The allelic frequency was dominant for the arginine-encoding allele compared to the proline-encoding allele (* vs. **; $P = 0.0405$).
[1]Unknown due to complete deletion.

mRNA and protein. Mutated cell lines clustered into two areas, B and C; missense mutated cell lines fell into cluster B, and cell lines with mutations other than missense mutations (non-missense mutated cells) fell into cluster C. Thus, mutated cells were subdivided into two groups characterized by different imbalances in expression patterns between the transcript and protein levels because of mutations.

The *mdm2* mRNA levels also failed to correlate with either the *p53* mRNA ($r = 0.256$, $P = 0.152$) or protein ($r = 0.1059$, $P = 0.409$) levels. Differences in expression levels between wild-type and mutated cell lines were found only for *p53* mRNA, but not for p53 protein or *mdm2* mRNA. However, among the three groups of wild-type, missense mutated, and non-missense mutated cell lines, the association with *p53* mutational status was the highest for p53 protein levels, followed by *p53* mRNA levels, and then *mdm2* mRNA levels ($P = 0.0033$ vs. 0.0042 vs. 0.081, Kruskal–Wallis test).

Table 3 Comparison of total p53 protein concentration and the degree of p53 activation induced by Nutlin-3 in the various cell lines

		Nutlin-Induced p53 activation		
	p53 protein (ng/ml)[1]	DNA-binding capacity (induction fold)[2]	Phospho-p53^{ser15} (induction fold)[2]	Apoptosis (degree)[3]
Wild-type cells				
ST1	1.59	15.0	16.3	++
KOB	5.47	2.5	4.2	+
LM-Y1	3.82	3.9	6.1	+
OMT	5.85	2.8	19.8	+
MT2	2.58	3.5	8.9	+
HUt102	2.21	4.5	20.9	+
MOLt4	1.65	14.7	19.6	+
SuDHL	3.92	5.1	12.5	++
HS-Sultan	8.65	nt	nt	–
Mutant cells with missense				
KK1	5.23	2.2	0.8	+/–
Ramos	10.17	1.4	1.2	–
MT1s	1.17	10.7	11.8	+
SO4	15.00	2.4	1.5	–
Mutant cells without missense				
Jurkat	0.44	<0.1	<0.5	–
THP1	0.06	NC	NC	–
U937	0.26	NC	NC	–
HL60	0.07	NC	NC	–
K562	0.07	NC	NC	–

NC, no change in fold induction.

[1]The p53 protein concentration was displayed as pg/10 μg cell lysates.

[2]The degree of the DNA-binding and phospho-p53^{ser15} capacity was scored as induction fold relative to the measures before and after treatment with Nutlin-3.

[3]Apoptotic cells assessed as cells staining for annexin-V and propidium iodide (++, 50% or more; +, 10–50%; ±, 10% or less).

Analysis of p53 activation induced by Nutlin-3

To analyze, the activation of p53 aberrantly expressed in the cell lines, a transcription factor assay was performed as a marker of the DNA-binding capacity and the phosphorylation assay was performed to detect p53^{ser15}. These assays showed characteristic results specific for each group, classified according to the type of mutations, as summarized in Table 3. In wild-type cell lines, p53 was expressed at intermediate levels, and the DNA-binding and phosphorylation capacity of p53 were evident, leading to apoptosis after treatment with Nutlin-3. However, although missense mutated cell lines expressed high levels of p53 protein, the DNA-binding and phosphorylation capacities were poor and apoptotic induction varied, indicating that the quantity and function of missense mutated p53 were not associated. In non-missense mutated cell lines, p53 protein was rarely detected, and p53 activation and apoptosis were not induced.

Discussion

p53 mutations currently have the distinction of being the commonest mutations found in human cancers, including hematologic malignancies. *p53* is a tumor suppressor gene and inactivation of *p53* function is a causative event in oncogenesis.

This study analyzed *p53* mutational status in the entire ORF, and the types of mutations were related to the quantitative expression of *p53* mRNA and protein in 22 hematopoietic cell lines. The results showed that half of the cell lines harbored *p53* mutations and that the mutations occurred preferentially in arginine-encoding alleles of the *p53* codon 72 polymorphism. Notably, four of nine ATL-derived cell lines had carried p53 mutations on different sites with three missense and one silent. The p53 protein levels in mutated cells were not correlated with the levels of *p53* mRNA, and cells with missense mutations exclusively harbored over-expressed p53 proteins. Mutated p53 proteins, despite of over-expression, were defective for Nutlin-mediated activation and stabilization. These abnormalities in both the levels and functioning of the p53 protein depended on the type of mutations, and not solely on the presence of mutations.

The frequency of *p53* mutations found in these cell lines seems to be slightly higher than, or similar to, that found in primary hematologic malignancies, such as 39% in acute lymphoblastic leukemia, 44% in ATL, 32% in acute myelogenous leukemia, and 42% in chronic lymphocytic leukemia (16–18). Most mutations detected in this study were single nucleotide substitutions, being

mainly missense mutations, followed by deletion, insertion, nonsense, and silent mutations. About 90% of the mutations were located from amino acids 102 to 292, which contains the DNA-binding domain. Consistent with results on the *p53* codon 72 polymorphism involving in the dominant-negative function and cancer risk (19, 20), *p53* mutations found in cell lines in this study occurred preferentially in the arginine-encoding alleles. In contrast, the allelic frequency in the wild-type cell lines was almost the same as in Japanese controls; 0.55 (Arg) vs. 0.45 (Pro) in this study, and 0.58 and 0.42 in Japanese controls. These *p53* mutational profiles of hematologic cell lines are similar to the pattern found in primary malignant solid tumors and hematologic malignancies reported in the database by Prokocimer *et al.* (18).

MDM2 mediates the ubiquitin-dependent degradation of p53, enhancing tumorigenic potential and resistance to apoptosis. Our data showed that the resistance to Nutlin-mediated apoptosis was basically associated with the presence and type of p53 mutations, although there existed several exceptional cases, such as HS-Sultan and MT1s (Table 3). This means that many complicated factors alternative to MDM2-p53 interaction, such as anti-apoptotic inhibitors, ATM, single polymorphic gene, and so on, may be involved in the Nutlin-induced apoptosis. A unique association between *p53* mutational status and *p53* mRNA and protein expression levels, quantified by real-time RT-PCR and Luminex methods, was also demonstrated in this study. The expression levels of *p53* mRNA in mutated cell lines were lower than in wild-type cell lines, indicating that *p53* mRNA quantification is useful for detecting the presence or absence of mutations. The present data on *p53* mRNA quantification were similar to those reported by Baumbush *et al.* (21), whose data showed that the expression levels of *p53* mRNA were highest in mutated tumors with missense mutations, followed by wild-type tumors, and then mutated tumors with nonsense and deletion mutations. Although the *p53* mRNA levels quantified by RT-PCR seem to show a marked variability, the aberrant expression of *p53* mRNA in mutated cell lines seemed to be consistent. Mutated cell lines with missense mutations over-expressed p53 protein despite having lower mRNA expression levels than in wild-type cell lines. Recent studies have shown that the p53 protein levels do not necessarily correlate with p53 mRNA at the transcript level, even in normal cells, because of the short half-life of the wild-type p53 protein (1). This study found that p53 over-expression was closely associated with missense mutations, but was not correlated with *p53* mRNA or *mdm2* mRNA expression levels. This finding suggests that structural alterations of the mutant protein modulated by missense mutations may be involved in the degradation of the protein, through post-translational modification (22–24). However, cell lines with non-missense mutations had neither detectable levels of *p53* mRNA nor protein. This is probably explained by impairment of the pretranslational stage. Overall, this unique association implies that *p53* mutations can affect the expression levels and functioning of the p53 protein.

In conclusion, the results of this study suggest that the frequency of *p53* mutations in hematopoietic cell lines is 50%. They also demonstrate that a unique association exists between the *p53* mutational status and the expression levels and functioning of its mRNA and protein, which depended not only on the presence or absence of mutations but also on the type of mutation. The characteristics observed in mutated cell lines could act as biomarkers to allow the better understanding of *p53*-associated tumor biology, and for screening for *p53* status in clinical settings.

Acknowledgements

This study was supported financially by a Japanese national grant, Kakenn, No. 17390165.

Author's contribution

SK designed this study, interpreted the data, and wrote the manuscript. AU, TT, DS, HH, and KY carried out molecular experiments, and KT and YY supplied and maintained cell lines and interpreted the data.

Competing interests

The authors declare that they have no competing interests.

References

1. Lain S, Lane DP. Tumor suppressor genes. In: Knowles M, Selby P, eds. *Introduction to the Cellular and Molecular Biology of Cancer*. Oxford: Oxford Press, 2005:135–55.
2. Poeta ML, Manola J, Goldwasser MA, *et al.* TP53 mutations and survivin in squamous-cell carcinoma of the head and neck. *N Eng J Med* 2007;**357**:2552–61.
3. Quon KC, Berns A. Haplo-insufficiency? Let me count the way. *Genes Dev* 2001;**2**:113–23.
4. Soussi T, Asselain B, Hamroun D, Kato S, Ishioka C, Claustres M, Beroud V. Meta-analysis of the *p53* mutation database for mutant *p53* biological activity reveals a methodological bias in mutation detection. *Clin Cancer Res* 2006;**12**:62–9.
5. Thomas M, Kalita A, Labrecque S, Pim D, Banks L, Matlashewski G. Two polymorphic variants of wild-type p53 differ biochemically and biologically. *Cell Mol Biol* 1999;**19**:1029–100.